

Calculation of Viscous Effects on Ship Wave Resistance Using Axisymmetric Boundary Layer Approaches

HENRY T. WANG

*Fluid Dynamics Branch
Marine Technology Division*

May 13, 1985



NAVAL RESEARCH LABORATORY
Washington, D.C.

SECURITY CLASSIFICATION OF THIS PAGE

REPORT DOCUMENTATION PAGE				
1a. REPORT SECURITY CLASSIFICATION UNCLASSIFIED		1b. RESTRICTIVE MARKINGS		
2a. SECURITY CLASSIFICATION AUTHORITY		3. DISTRIBUTION / AVAILABILITY OF REPORT Approved for public release; distribution unlimited.		
2b. DECLASSIFICATION / DOWNGRADING SCHEDULE				
4. PERFORMING ORGANIZATION REPORT NUMBER(S) NRL Report 8881		5. MONITORING ORGANIZATION REPORT NUMBER(S)		
6a. NAME OF PERFORMING ORGANIZATION Naval Research Laboratory	6b. OFFICE SYMBOL (If applicable) Code 5841	7a. NAME OF MONITORING ORGANIZATION Office of Naval Research		
6c. ADDRESS (City, State, and ZIP Code) Washington, DC 20375-5000		7b. ADDRESS (City, State, and ZIP Code) Arlington, VA 22217		
8a. NAME OF FUNDING / SPONSORING ORGANIZATION Office of Naval Research	8b. OFFICE SYMBOL (If applicable)	9. PROCUREMENT INSTRUMENT IDENTIFICATION NUMBER		
8c. ADDRESS (City, State, and ZIP Code) Arlington, VA 22217		10. SOURCE OF FUNDING NUMBERS		
		PROGRAM ELEMENT NO. 61153N	PROJECT NO.	TASK NO.
				WORK UNIT ACCESSION NO. DN280-006
11. TITLE (Include Security Classification) Calculation of Viscous Effects on Ship Wave Resistance Using Axisymmetric Boundary Layer Approaches				
12. PERSONAL AUTHOR(S) Wang, Henry T.				
13a. TYPE OF REPORT Interim	13b. TIME COVERED FROM 1/84 TO 12/84	14. DATE OF REPORT (Year, Month, Day) 1985 May 13	15. PAGE COUNT 44	
16. SUPPLEMENTARY NOTATION				
17. COSATI CODES			18. SUBJECT TERMS (Continue on reverse if necessary and identify by block number)	
FIELD	GROUP	SUB-GROUP	Ship wave resistance Viscous effects	
			Axisymmetric boundary layer	
			Ship hulls	
19. ABSTRACT (Continue on reverse if necessary and identify by block number)				
<p>This report investigates the effect of fluid viscosity on ship wave resistance for a wide range of ship hulls. Two direct, simple models are used to model the potential flow around the hull: Michell thin-ship theory and zeroth order slender ship theory. The viscous flow is modeled by two relatively simple integral boundary layer methods, both of which approximate the actual hull by axisymmetric bodies. The various methods are used to calculate wave resistance for a series of speeds for five ship hulls, three of which have extensive experimental data. The results basically show that the trend of the viscous correction is to improve the agreement of the calculated and measured values. For the thicker ship hull cases, the results indicate that a more complex potential flow wave resistance theory is required to obtain reasonable agreement with measured results.</p>				
20. DISTRIBUTION / AVAILABILITY OF ABSTRACT <input type="checkbox"/> UNCLASSIFIED/UNLIMITED <input checked="" type="checkbox"/> SAME AS RPT. <input type="checkbox"/> DTIC USERS		21. ABSTRACT SECURITY CLASSIFICATION UNCLASSIFIED		
22a. NAME OF RESPONSIBLE INDIVIDUAL Henry T. Wang		22b. TELEPHONE (Include Area Code) (202)767-2516	22c. OFFICE SYMBOL Code 5841	

DD FORM 1473, 84 MAR

83 APR edition may be used until exhausted.
All other editions are obsolete.

SECURITY CLASSIFICATION OF THIS PAGE

CONTENTS

INTRODUCTION	1
FORMULATION OF THE WAVE RESISTANCE PROBLEM	2
PREVIOUS STUDIES	3
Potential Flow	3
Stern Boundary Layer Flow	5
PRESENT CALCULATION PROCEDURES	7
Potential Flow Calculation	7
Boundary Layer Calculation	8
Equivalent Axisymmetric Bodies	8
Momentum Integral Equation	8
Choice of Initial Conditions	10
Calculation of Pressure Distribution on Body Surface	11
Computerized Calculation Procedure	13
DESCRIPTION OF SHIP HULLS	14
Choice of Ship Hulls	14
Geometric Characteristics of Ship Hulls	14
RESULTS	17
Matrix of Computer Runs	17
Calculated Results	18
DISCUSSION OF RESULTS	31
Equivalent Bodies of Revolution	31
Boundary Layer Modification to Source Strength	31
Wigley Hull	32
Series 60 Hull	33
Sharma Strut	33
EP Strut (Elliptic Bow-Parabolic Stern, $B/L = 0.15$)	34
TEP Strut (Thin Elliptic Bow-Parabolic Stern, $B/L = 0.05$)	34
Overall Trends	35
SUMMARY AND CONCLUSION	35
Calculation Approach	35
Hull Selection	36
Calculated Results	36
REFERENCES	37

CALCULATION OF VISCOUS EFFECTS ON SHIP WAVE RESISTANCE USING AXISYMMETRIC BOUNDARY LAYER APPROACHES

INTRODUCTION

An historic paper by Michell [1] developed a direct calculation procedure based on thin-ship theory. Since then, calculation of the resistance due to the waves generated by a surface ship advancing at constant forward speed has been an area of active interest. Several international seminars and workshops on wave resistance have been held in recent years. The accurate calculation of the wave resistance is important for commercial as well as Navy ships since it is one of the major components of overall drag. In addition, since the wave resistance represents a particular weighted integral of the amplitude spectrum of the waves, its accuracy also gives an indirect indication of the overall accuracy of the calculated shape of the wave spectrum in wave number space and the associated wave pattern on the physical free surface.

Most of the efforts aimed at improving the agreement of the calculated and measured results have centered along two distinct lines. In one approach, potential flow is assumed; efforts are made to better satisfy the kinematic condition on the hull surface and the nonlinear dynamic condition on the unknown free surface. Due to the complexity of free surface flows, these efforts often lead to calculation procedures which are orders of magnitude more time-consuming than the original Michell approach. In the other approach, the assumption of potential flow is removed, and attempts are made to account for the effect of fluid viscosity on the flow near the ship. The usual procedure is to take the viscous flow to effectively change the shape of the ship in the stern and near-wake regions. The proposed calculation procedures have ranged from the use of empirical correction factors or the assumption of plausible mathematical shapes to the use of complex and time-consuming higher order boundary layer theory. The effect of the resultant change in hull shape on the calculated wave resistance is often assessed by using the original thin-ship theory.

This report investigates the effect of fluid viscosity for a scope which is wider than that of previous studies. Two direct, simple models are used to model the potential flow: the previously mentioned Michell thin-ship theory, and zeroth order slender-ship theory, as it is termed by Noblesse [2]. The viscous flow is modeled by two relatively simple, integral boundary layer methods, both of which approximate the actual hull by axisymmetric bodies. One method tends to overestimate the viscous effects while the other tends to underestimate these effects. The various methods are used to calculate wave resistance for a series of speeds for five ship hulls, three of which have extensive experimental data. The fourth hull illustrates a case where the present simple methods basically break down; the fifth hull illustrates the effects of viscosity for an unsymmetrical ship moving in both forward and backward directions. The entire calculation procedure is simple enough to run with ease on a minicomputer.

The report starts with a statement of the formulation of the wave resistance problem and a brief review of the various calculation methods used in the potential and viscous flow areas. The review is not comprehensive but indicates the principal approaches in each area. A description is next given of the relatively simple potential flow and axisymmetric boundary layer methods used in the present study. Their limitations and likely accuracy are discussed. The major geometrical features of the five ship

hulls considered in the present study are given. The calculated boundary layer parameters, as well as the calculated and measured values of wave resistance, are presented in tabular and graphic forms. The calculated values of wave resistance with viscous correction effects are compared with corresponding potential flow results and with measured values. The report concludes with a summary of the principal results.

FORMULATION OF THE WAVE RESISTANCE PROBLEM

The problem is usually formulated for a coordinate system fixed to the ship. Figure 1 shows the coordinate system used in the present study, with origin at the forward perpendicular, x positive from stern to bow, y positive to port, and z positive upwards. The figure also defines terms for the ship configuration which will be used throughout this report. In this coordinate system, the flow pattern is steady with uniform flow velocity U in the negative x -direction as $x \rightarrow +\infty$. The assumptions are usually made that the fluid is inviscid and incompressible, the flow is irrotational, and surface tension effects may be neglected. Refinements to account for viscous effects, which are important in the stern and near wake, are discussed later. Surface tension effects are important only for waves of small wavelength, such as capillary waves.

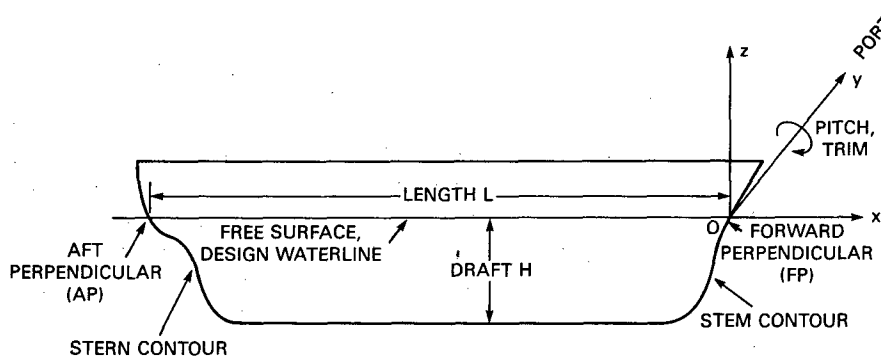


Fig. 1 — Ship configuration and coordinate system

Under the above assumptions, the flow field is described by the velocity potential $\Phi(x,y,z)$ which satisfies Laplace's equation

$$\nabla^2 \Phi = 0. \quad (1)$$

On the free surface $z = \zeta(x,y)$, the dynamic and kinematic boundary conditions are respectively given by

$$g \zeta + \frac{1}{2} (\nabla \Phi)^2 = \frac{1}{2} U^2 \quad (2)$$

and

$$\frac{d}{dt} (z - \zeta) = \nabla \Phi \cdot \nabla (z - \zeta) = \Phi_x \zeta_x + \Phi_y \zeta_y - \Phi_z = 0 \quad (3)$$

where g is the gravity constant and t is time. The combination of the dynamic and kinematic conditions gives

$$g \Phi_z + \nabla \Phi \cdot \nabla \left[\frac{1}{2} (\nabla \Phi)^2 \right] = 0 \quad \text{on } z = \zeta(x,y). \quad (4)$$

The kinematic boundary condition on the wetted ship hull S_H is that no fluid goes through the ship hull

$$\vec{n} \cdot \nabla \Phi = 0 \quad \text{on } S_H \quad (5)$$

where \vec{n} is the inward normal to the ship hull. Finally, the radiation condition states that waves are not radiated upstream.

Once Φ is obtained, the wave resistance D_W may be obtained by direct integration of the pressure p acting on the hull surface S_H

$$D_W = \int \int_{S_H} p n_x \, ds \quad (6)$$

where n_x is the x -component of the inward normal to the hull, and p is related to Φ by Bernoulli's equation

$$p = -\frac{\rho}{2} [(\nabla \Phi)^2 - U^2] - \rho g z \quad (7)$$

where ρ is the fluid density.

In the above form, the calculation of D_W requires the evaluation of gradients of Φ , which tends to accentuate inaccuracies in Φ . An alternate, more commonly used, approach is to relate the wave resistance to the energy flux of the generated waves across a vertical plane, $x = \text{constant}$, downstream of the ship. Following the derivation given, for example in Refs. 3 or 4, the following expression for D_W in terms of the amplitude spectrum $A^2(\theta)$ is obtained

$$D_W = \frac{1}{2} \pi \rho U^2 \int_{-\pi/2}^{\pi/2} A^2(\theta) \cos^3 \theta \, d\theta \quad (8)$$

where θ is the angle of direction of propagation with respect to the x -axis of the component wave. For the usual case where Φ is represented by a distribution of sources over the hull surface, it is further shown in Ref. 4 that $A^2(\theta)$ is given by an integral of the source densities over the hull surface weighted by a wave elevation function.

Equation (8) shows that the wave resistance represents an integrated average of the amplitude spectrum weighted by the factor $\cos^3 \theta$. This means that the wave resistance is dominated by the transverse waves, for which $|\theta| < 35^\circ$. Using the relations given in Ref. 4, the amplitude spectrum can be alternatively expressed as a single function of the wavenumbers in the x or y directions, respectively k_x and k_y . These relations in terms of k_x or k_y would be useful in obtaining wave resistance from a longitudinal or lateral wave cut.

PREVIOUS STUDIES

Potential Flow

The Proceedings of the Workshop on Ship Wave-Resistance Computations [5] gives numerous examples of recent approaches for solving the above problem. Relatively few studies attempt to directly solve the problem, which includes the application of the nonlinear free surface condition (Eq. (4)) on the unknown free surface $z = \zeta$. Chan and Chan [6,7] obtain the steady state solution by marching forward in time and using a finite difference grid to model the flow field. Their approach is unsuitable for the calculation of the wave resistance since the solution must be solved for a number of time steps until the steady state solution is reached. Von Kerczek and Salvesen [8-10] also use a finite difference approach to solve the flow around prescribed isolated and distributed singularities. However, their work is restricted to two-dimensional flow. At a somewhat lower level of complexity, coordinate transformation techniques may be used to transform the physical coordinate system into a new coordinate system where the free surface is known. The actual nonlinear problem is converted to a series of linearized problems on the successively iterated free surface. Two methods which have been used are Guilloton's method [11,12] where lines of constant pressure become constant coordinate lines, and a Lagrangian method [13] where streamlines become constant coordinate lines.

The majority of studies consider only the linearized form of Eq. (4) and apply this condition on the undisturbed free surface $z = 0$ instead of on $z = \zeta$. Since the disturbances to the free surface are considered to be small, it is convenient to express the total potential Φ as the sum of a base flow potential ϕ_B and a perturbation potential ϕ ; here

$$\Phi = \phi_B + \phi. \quad (9)$$

The base flow is usually taken to be uniform flow, for which

$$\phi_B = -Ux, \quad (10a)$$

or the flow around the ship hull where the free surface is taken to be a horizontal plane of symmetry, for which

$$\phi_B = \phi_D. \quad (10b)$$

The latter case is often referred to as double model flow and may be viewed as the limiting case of velocities U which are slow enough that the free surface is undisturbed. If the base flow potential is given by Eq. (10a), the linearized form of the free surface condition, Eq. (4), is

$$g\phi_z + U^2\phi_{xx} = 0 \quad (11)$$

and the hull boundary condition, Eq. (5), becomes

$$\vec{n} \cdot \nabla\Phi = Un_x. \quad (12)$$

Two computer methods developed by Chang [14] and Dawson [15] are representative of the approaches used to solve the above (linearized) problem. Chang divides the ship into a series of quadrilaterals, on each of which is placed a Kelvin (or Havelock) source of uniform but unknown density σ . The Green function for the Kelvin source G [16,17] may be written as

$$G = \frac{1}{r} - \frac{1}{r_1} + G_2. \quad (13)$$

The first term is simply the potential for a Rankine (infinite fluid) source placed on the ship hull $(x_0, y_0, -z_0)$. The second term is the potential for a Rankine sink placed at $(x_0, y_0, +z_0)$. The third term is a double integral which gives the wave disturbance due to an oscillating source placed below a linearized free surface. Since the Kelvin source is specifically constructed to satisfy the linearized free surface condition (Eq. (11)) and the radiation condition, the hull boundary condition (Eq. (12)) results in a series of algebraic equations for the unknown source strengths σ . The principal difficulty in this approach is the careful evaluation of the matrix of velocity influence coefficients due to the complex Havelock sources. Also, matrix inversion techniques must be used to solve the resulting set of algebraic equations. The type of problem solved by the Chang approach is commonly called the Neumann-Kelvin problem.

Dawson uses a different approach which avoids the above difficulty involving the use of Havelock sources. He linearizes the free surface condition (Eq. (4)) by using the double model flow as the known base flow, resulting in

$$\phi_{Dl}^2\phi_{Dll} + (\phi_D^2\phi_l)_l + g\phi_z = 0 \quad (14)$$

where l denotes differentiation along a streamline of the flow. He divides the actual ship hull, its reflection above the undisturbed free surface, and the undisturbed free surface adjacent to the hull into a series of quadrilaterals. He places a Rankine (infinite fluid) source of uniform but unknown density on each quadrilateral. The kinematic hull condition (Eq. (5)) is used for the quadrilaterals on the hull and its reflection. The free surface condition (Eq. (14)) expressed in finite difference form, is used for the quadrilaterals on the free surface near the hull. A four-point difference operator is found to approximately satisfy the radiation condition in that upstream waves are suppressed. The resulting set of algebraic equations can then be solved for the strength σ of the source on each quadrilateral. One of

the principal difficulties of this approach is that panels must be used to model not only the actual hull but also its reflection and part of the free surface. Also, great care must be exercised in choosing the proper extent of the free surface and the manner of application of the free surface condition.

The above shows that the solution of even the linearized problem is a rather formidable task. The solution can be simplified considerably if the beam B and draft H are small compared to the ship length and the dominant length U/\sqrt{g} of the generated waves so that the disturbance potential ϕ can be considered negligibly small compared to the base flow potential ϕ_B . In this case, termed zeroth order slender-ship theory by Noblesse [2], the source strength σ can be directly obtained from the geometry of the hull

$$\sigma(x,y,z) = \frac{-U}{4\pi} n_x = \frac{-U}{4\pi} \left[\frac{+\partial f/\partial x}{\sqrt{1 + (\partial f/\partial x)^2 + (\partial f/\partial z)^2}} \right] \quad (15)$$

where $f(x,z)$ is the local half-width of the ship. The resulting direct expression for the perturbation potential ϕ is given by two integrals which are entirely dependent on ship geometry:

$$\phi = \int_{S_H} \sigma G ds + F_n^2 \int_C \sigma n_x \tau_y \sigma G dl, \quad (16)$$

where $F_n = U/\sqrt{gL}$ is the Froude number,
 C is the waterline contour of the ship, and
 τ_y is the y -component of the tangent to the waterline contour.

Noblesse shows that a series of higher order slender-ship solutions may be obtained by an iterative procedure whereby the n th order solution is obtained as a perturbation to the uniform base flow plus the $(n-1)$ st order solution. Thus, the above zeroth order solution is the perturbation to the base flow only, neglecting any flow caused by motion of the ship. On the other hand, the first order solution would be the perturbation to the base flow plus the above zeroth order solution. In the remainder of this report, the zeroth order solution given by Eqs. (15) and (16) will simply be referred to as slender-ship theory.

A further simplification occurs if the beam of the ship is also assumed to be small compared to draft, as well as the previously mentioned ship and wave lengths, resulting in the Michell thin-ship theory. In this case, the surface integral in Eq. (16) is calculated over the centerplane S_0 instead of the actual hull surface S_H , and the contour integral is negligibly small. Also, the terms involving $(\partial f/\partial x)^2$ and $(\partial f/\partial z)^2$ in Eq. (12) are neglected. Equations (12) and (13) then respectively become

$$\sigma(x,z) = \frac{-2U}{4\pi} \frac{\partial f}{\partial x} \quad (17)$$

and

$$\phi = \int_{S_0} \sigma G ds \quad (18)$$

where the factor 2 in Eq. (17) indicates that both sides of the ship hull, assumed to have port and starboard symmetry, are collapsed onto the centerplane.

Stern Boundary Layer Flow

The viscous boundary layer in the stern region is usually of sufficient thickness to significantly influence the flow around the ship. An indication of the importance of the viscous flow is that several characteristic differences exist between the wave resistance values calculated using methods which neglect the effects of viscosity and measured results. The largest difference is that measured results show reduced amplitudes of variation with the Froude number compared to theoretical values. A second difference is that the location of the humps and hollows of the wave resistance curve for measured values tend to be shifted to higher Froude numbers.

Qualitatively, the boundary layer may be viewed as essentially thickening the width of the ship, leading to smaller magnitudes of the slope $\partial f/\partial x$ in the stern region. This in turn means a reduction in the strength and wave-making ability of the sinks located in the stern region. Thus, the earliest efforts at accounting for the effect of viscosity centered on finding simple or empirical expressions for this reduction. Havelock [18] found that a constant reducing factor of $\beta = 0.6$ for the sink strengths over the rear half of the ship significantly reduced the amplitude of oscillation of the wave resistance curve. Wigley [19] deduced from experiments the following reducing factor $1 - \beta_\omega^2$ for the wave resistance of the after-body of the ship:

$$1 - \beta_\omega^2 = 1 - e^{-0.001/F_n^5}. \quad (19)$$

This shows that the wave resistance reducing factor $1 - \beta_\omega^2$ is largest at small F_n and approaches 0 (i.e., no reduction) as F_n increases.

Later efforts centered on the effect of different assumptions of stern and near wake shapes on the wave resistance curve. Havelock [20] and Milgram [21] make parametric studies of the effect of different shape modifications in the stern-near wake region on the wave resistance curve. They both assume that the boundary layer is negligibly thin up to a certain "separation" point on the aft body. Downstream of this point, a mathematical form (with thickness and slope equal to that of the actual hull at the separation point) is assumed. Milgram assumes a form which has zero slope from the aft, perpendicular to infinity. This leaves an open wake of constant width aft of the ship. Havelock assumes a quartic (or cubic) curve which has zero slope and zero (or nearly zero) thickness at various selected distances behind the ship. This gives rise to a wake of zero (or small) thickness beyond this point. In both studies, the amplitude of oscillation of the wave resistance curve tends to decrease with forward positioning of the separation point.

The above studies are largely concerned with giving overall trends of the possible effect of viscous flow on wave resistance. As such, they cannot be expected to yield accurate results for a particular ship. More recent studies have largely used either low order boundary layer theory or experimental measurements to obtain the displacement thickness δ^* . This is then added to the stern and near wake region of the ship, resulting in an effectively thicker and longer ship. The earliest attempts along these lines are those by Wigley [22] and Wu [23] who use two-dimensional boundary layer theory to calculate δ^* up to the aft perpendicular. For the wake region, Wigley uses an approach similar to the previously mentioned Havelock [20] approach to obtain a closed (or nearly closed) wake at a certain distance behind the ship. He shows that the calculated wave resistance is sensitive to the wake distance but gives no guidelines for its choice. Wu mentions various ways of treating the wake region but essentially leaves it out in his numerical examples.

Himeno [24], Kinoshita [25], and Larsson and Chang [26] make rather comprehensive studies of the effect of different boundary layer and wake approximations on the calculated wave resistance for particular ship forms. Himeno uses three-dimensional integral boundary layer theory to calculate the tangent and cross flows along the streamlines. He uses Michell thin-ship theory to calculate the wave resistance, with and without viscous effects, for the Series 60, $C_B = 0.70$ form. He finds that the wave resistance curve, for the case where only the displacement thickness for tangential flow is included, gives an appreciable attenuation of the hollows and bumps at low Froude numbers. However, the wave resistance curve for the more complete case where displacement thicknesses for both tangential and cross flows are included, has pronounced hollows and humps and is in general higher than the corresponding curve with no viscous corrections. This, of course, is contrary to the trend for most measured cases.

Kinoshita [25] gives an estimate of the various effects of viscous flow on wave resistance. His main conclusion is that the effect on wave propagation and the effect due to the rotational flow of the wake are small compared to the deformation of the potential flow, as modeled by the displacement thickness. He uses measured boundary layer velocity distributions to obtain the displacement thickness

along the hull and in the wake. His results for a thin strut show that the inclusion of the measured displacement thicknesses moves the Michell wave resistance curve into substantially good agreement with measured values. His results also show the interesting trend that there is relatively little difference in the wave-resistance values for the case where δ^* is assumed to be constant with depth and the more realistic case where δ^* varies with depth.

Larsson and Chang [26] use higher-order boundary layer theory to calculate the displacement thickness along the hull and in the near wake for the Series 60, $C_B = 0.70$ ship form used by Himeno [24]. They make wave-resistance calculations using Michell thin-ship theory as well as the method by Chang [14], using the more complex Neumann-Kelvin approach given by Eqs. (9)-(13). For the thin-ship case, they make calculations for the wake terminating at the aft perpendicular (leading to a relatively large open wake) as well as using a calculated wake; this results in a narrower but still open displacement body aft of the ship. Even though no experimental data are shown, several important points may be deduced from their calculated results. First, there is relatively good agreement between the calculated results, neglecting viscous effects, using the thin-ship and Neumann-Kelvin approaches. Secondly, the effect of the viscous correction is to lower the wave resistance in all cases. Thirdly, the reduction in wave resistance is greater for the narrower wake, but the difference in the reduction between the two wakes varies with Froude number. They show that thin-ship theory, when applied to an open wake, does not properly account for the contribution of the transverse wave system to the wave resistance. Thus, when the drag due to the transverse waves is dominant, there is a large difference in the calculated reduction between the two wakes. On the other hand, the difference is small when the divergent waves are dominant. It is of interest to note that in spite of their observation concerning the open wake, their viscous flow calculation procedure still leaves an open wake aft of the ship.

PRESENT CALCULATION PROCEDURES

Potential Flow Calculation

Largely due to the simplicity of the direct solution methods, it was decided to use slender-ship and Michell thin-ship theories to make the wave resistance calculations. These theories are respectively given by Eqs. (15)-(16) and Eqs. (17)-(18). Use of these simple theories allows calculation of wave resistance, with and without viscous correction, for a wider range of ship hull cases than in previous studies. Also, the preceding discussion of previous studies shows that in many cases the viscous flow correction is as important as higher order potential flow theory in bringing the calculated results into better agreement with measured values.

The thin-ship calculations are made using a computer program developed by Chapman [27], based on the method outlined in Ref. 4. Briefly, the ship centerplane is divided into a series of quadrilaterals or triangles, on each of which is placed a source of constant strength σ , given by Eq. (17). The program then computes an amplitude spectrum A^2 for the far-field waves as a function of the longitudinal wave number k_x by integrating the product of σ and essentially the far-field wave part of the Kelvin source G given in Eq. (13). The wave resistance is then calculated by using an equation similar to Eq. (8), with the exception that the independent variable is now k_x instead of θ . Reference 4 shows that the amplitude spectrum can be expressed as a single function in terms of k_x , θ , or k_y , the lateral wave number. It may also be noted that the wave elevation on the free surface, $\zeta(x,y)$, may be conveniently obtained from the amplitude spectrum by using Fourier transform methods.

Two extensions were added to the program to upgrade it to slender-ship capability. First, the calculation of the line integral in Eq. (16) was added to the program in the form of a subroutine. Secondly, a geometry subroutine [28] was added to calculate average values of n_x in Eq. (15) over a ship panel. An additional consideration is that the ship panels are now placed over the actual hull surface S_H , instead of the centerplane S_0 , since the surface integral in Eq. (16) is now over S_H .

The modifications have been made in such a manner that the use of thin-ship or slender-ship theory is at the option of the user. The program also provides the option of modifying the hull surface to account for the displacement thickness which is calculated by the boundary layer methods described below.

Boundary Layer Calculation

The results of the previous studies indicate two principal points. First, the wave resistance is sensitive to the shape of the wake aft of the ship. The discussion in Ref. 26 indicates that an open wake will tend to overestimate the wave resistance, with the error depending on the relative importance of the transverse waves. However, the results of Ref. 22 indicate that closing the wake arbitrarily may lead to increases in wave resistance. Except for those cases where the wake is mathematically shaped, the wake usually has been open. Secondly, the results of Refs. 24 and 25 indicate that more careful modeling or calculation of the boundary layer effects need not lead to wave resistance values which are in better agreement with experimental results.

In view of the above, and the simplicity of the methods chosen to make the wave resistance calculations, it was decided to use a relatively simple, axisymmetric momentum-integral boundary layer method to model the overall characteristics of the viscous flow on the ship hull. Following the suggestion by Granville [29], the actual hull is approximated by an axisymmetric body, as described below. This axisymmetric approach does not appear to have been used in previous studies which investigated the effect of viscosity on wave resistance. These studies have largely used two- and three-dimensional theories. Because of the complexity and uncertainty surrounding the near-wake flow, the boundary layer calculations are terminated at the aft perpendicular. This leaves an open wake which may overestimate the wave resistance (i.e., underestimate the reduction due to viscous flow) for certain Froude number cases.

Equivalent Axisymmetric Bodies

In the present approach, the three-dimensional hull is replaced by an equivalent axisymmetric body. Two possibilities exist: respectively equal in volume, and wetted area to a double model of the hull, which is defined as the underwater portion of the ship and its reflection about the free surface, taken to be horizontal. At a given longitudinal station x , the radii of the equal volume and equal wetted area bodies, respectively R_V and R_W , are given by Ref. 29 as

$$R_V = \sqrt{\frac{2A(x)}{\pi}} \quad (20)$$

and

$$R_W = \frac{2P(x)}{2\pi} \quad (21)$$

where $A(x)$ is the cross-sectional area of the underwater portion of the ship, and $P(x)$ is the perimeter of the underwater portion of the ship.

Following Ref. 29, the pressure field is calculated by using the R_V body since it models the volume change along the actual hull. The boundary layer calculations are carried out using both bodies. It is pointed out later that the use of the two bodies tends to bracket the effect of streamline convergence obtained by more complex boundary layer methods.

Momentum Integral Equation

The momentum integral equation for boundary layer flow along an axisymmetric body may be conveniently derived from the more general three-dimensional formulation for flow along the ship hull.

In the more general approach, typically a series of streamlines are calculated along the hull surface. Then two momentum integral equations are integrated for tangential flow and cross flow along each streamline. If one assumes all cross flow terms, as well as derivatives normal to the streamlines, as being of higher order and considers the equation for tangential flow for a single representative streamline, the axisymmetric momentum integral equation [30] is obtained

$$\frac{d\theta}{ds} = \frac{C_f}{2} - (H + 2) \frac{\theta}{U_e} \frac{dU_e}{ds} - \frac{\theta}{R} \frac{dR}{ds}. \quad (22)$$

Here, $\theta = \int_0^\delta \left(1 - \frac{u}{U_e}\right) \frac{u}{U_e} d\lambda$ is the momentum thickness, (23a)

δ is the boundary layer thickness where $\frac{u}{U_e} = 0.995$,

u is the velocity in the boundary layer,

U_e is the velocity at the edge of the boundary layer,

s is the arc length measured on the body, starting from the bow,

$C_f = \tau_w / \frac{1}{2} \rho U_e^2$ is the skin-friction coefficient, (23b)

τ_w is the shear stress on the body surface,

$H = \delta^* / \theta$ is the shape parameter, (23c)

$\delta^* = \int_0^\delta \left(1 - \frac{u}{U_e}\right) d\lambda$ is the displacement thickness, and (23d)

R is the radius of the body.

Figure 2 shows the coordinate system used in the boundary layer calculations, where X is positive from bow to stern, contrary to the sense for x for the ship hull in Fig. 1. (This is because the boundary layer equation is integrated from bow to stern.) Effectively, calculations along a series of streamlines in the three-dimensional procedure are reduced to a single "average" streamline, namely the generating radius $R = R(x)$ of the axisymmetric body.

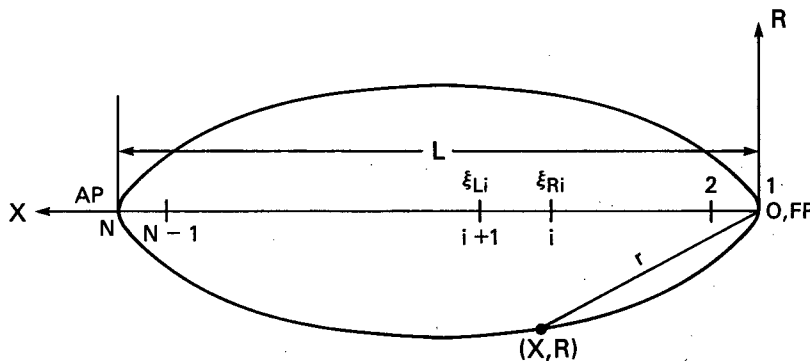


Fig. 2 — Axisymmetric body configuration and coordinate system

The three terms on the right hand side of Eq. (22) show that the boundary layer grows due to skin friction, adverse pressure gradient ($dU_e/ds < 0$), and streamline convergence ($dR/ds < 0$). Granville suggests that the pressure distribution be calculated by using the R_V equivalent body, and that the boundary layer growth be calculated by using the R_W equivalent body. This would tend to approximate the overall friction drag acting on the actual hull surface. However, it is not clear that the R_W body gives a better approximation to the streamline convergence term than the R_V body. Equations (20) and (21) show that in the case of a ship with a vertical stern contour of zero width, the case

for most of the ships considered in the present study, R_V and R_W take on the following values at the stern end

$$R_V = 0 \quad (24a)$$

and

$$R_W = \frac{4H}{\pi} \quad (24b)$$

where H is the draft of the actual ship. Consideration of the last term in Eq. (22) and Eq. (24) shows that the R_V body would tend to have a significantly larger streamline convergence effect than the R_W body. In fact, it will be shown later (in Fig. 4) that the values of dR/ds for the R_W body tend to have small magnitudes, giving rise to weak streamline convergence effects. If the streamlines on the hull are traced according to strict potential flow theory, they would all converge to a single stagnation point at the aft perpendicular. However, due to viscous flow, this stagnation point does not exist. Also, if one uses a numerical method where the ship surface is represented by a series of panels, the approximate nature of the calculation leads to the traced streamlines at the stern showing definite convergence, but not to a point [31-33]. The actual average streamline convergence behavior would tend to lie between those corresponding to the R_V and R_W bodies. Thus, to bracket the actual effect, boundary layer calculations were made using both equivalent bodies.

Taking the distribution of U_e to be known (this calculation will be described below), two additional equations are required to solve for the 3 unknowns θ , C_f , and H in Eq. (22). The two additional equations were taken to be the well-known Ludwig-Tillmann friction relation [34] and the entrainment equation of Head [35] and Standen [36]:

$$C_f = 0.246 \times 10^{-0.678H} R_\theta^{-0.268} \quad (25)$$

and

$$\frac{d}{ds} (\theta G) + \theta G \left(\frac{1}{U_e} \frac{dU_e}{ds} + \frac{1}{R} \frac{dR}{ds} \right) = F(G), \quad (26a)$$

$$G = 1.535 (H - 0.7)^{-2.715} + 3.3, \quad (26b)$$

and

$$F(G) = 0.0306 (G - 3.0)^{-0.653} \quad (26c)$$

where $R_\theta = U\theta/\nu$ is the Reynolds number based on momentum thickness (26d) and ν is the fluid kinematic viscosity. Equations (22) and (26) may be viewed as two equations for the two unknowns θ and H , with Eq. (25) furnishing an expression for C_f which appears in Eq. (22).

A more complex formulation for C_f suggested by Granville [37] and used in Ref. 33 was also tried for several cases. It was found that in nearly all cases, there was little difference between the two formulations in the calculated values for the displacement thickness δ^* , the boundary layer variable of principal interest in the present study.

Choice of Initial Conditions

An important and nontrivial part in boundary layer calculations is the choice of initial point s and starting values for the dependent variables θ and H . For cases where the calculations are made for a particular body for which experimental data are available, the convenient procedure is to use measured values of θ and H at a given initial station s_0 to start the calculations. This procedure is not possible for the present generalized study where a wide range of ship cases are considered. A second possibility is to use the straightforward approach outlined by Garcia and Zazurca [38]. They give a simple formula

for the growth of θ^2 of the laminar boundary layer in the bow region as well as various formulations for the location of transition, after which the turbulent boundary layer formulation of Eqs. (22), (25), and (26) may be used. This approach, however, has the following limitations. In most model tests, turbulence stimulation devices are placed in the bow region. While this fixes the location of transition from laminar to turbulent flow, the resulting characteristics of the turbulent boundary layer are a complex function of the location, size, and shape of the device. For those cases where no stimulation devices are used, the pressure gradient in the bow area often leads to a complex flow region of laminar separation with turbulent reattachment, which is not modeled by the above approach.

Consequently, the following, approximately uniform approach was used to make the parametric runs for the various ship cases described in the following chapter. The location of transition is fixed at a value of s_0 corresponding to $X/L = 0.05$, a typical location for turbulence stimulators used in model tests. The initial value of the momentum thickness θ_0 is set equal to 0.7 of the corresponding value for a flat plate with the same length Reynolds number, while the initial value of the shape factor H_0 is set equal to the flat plate value, usually in the 1.4 to 1.5 range. This was largely based on the results of Refs. 33, 39, and 40. These results show that the boundary layer thicknesses θ and δ^* in the bow region are usually somewhat smaller than flat plate values, due to the favorable pressure gradient and streamline divergence in this region, while H is typically 1.4. Numerical experimentation showed that in the case of the displacement thickness δ^* , different choices of θ_0 and H_0 led to differences in the bow region which tended to propagate unchanged to the stern region. These differences were quite small and essentially negligible compared to values of δ^* in the stern region where most of the boundary layer growth takes place due to the adverse pressure gradient and streamline convergence.

Calculation of Pressure Distribution on Body Surface

In the present thin-boundary layer approach, where the pressure is assumed to be constant throughout its thickness, the edge velocity U_e appearing in Eq. (22) is simply related to the pressure p on the body by Bernoulli's equation.

$$U_e = U \sqrt{1 - C_p} \quad (27)$$

where $C_p = (p - p_0) / \left(\frac{1}{2} \rho U^2 \right)$ is the pressure coefficient and p_0 is the ambient pressure far from the body.

There are well-known numerical procedures, such as the Hess and Smith method [41], for calculating the potential flow pressure distribution on arbitrary bodies of revolution to any desired degree of accuracy. While the method in Ref. 41 is straightforward, a number of numerical steps are involved, such as matrix inversion and calculation of elliptic integrals due to the use of ring sources on the body surface. In the present study, the simple and direct slender-body theory, as outlined by Karamcheti [42], is used to calculate the pressure distribution. The accuracy of the method is improved by using two modifications which are described later. In addition to its obvious simplicity, the present choice of calculation methods was also based on consideration of the pressure accuracy requirements at both ends of the body (where slender-body theory is most inaccurate). The approach for obtaining initial conditions for the boundary layer calculations described above essentially makes it unnecessary to have an accurate description of the pressure at the bow end. At the stern end, it is well-known that the potential flow pressure distribution is substantially modified by the viscous flow.

In conventional slender-body theory, the longitudinal axis of the body is divided into a series of $N - 1$ line segments of length ΔX_i , over each of which is placed a source of uniform density q_i , where ΔX_i and q_i may vary from segment to segment. The potential of the source G_s is given by

$$G_s = \frac{1}{r} = \frac{1}{\sqrt{(X - \xi)^2 + R^2}} \quad (28)$$

where ξ is a source point, between the ends of the i th line segment. The strength q_i is directly given by

$$q_i = \frac{U}{4\pi} \left(\frac{dA}{dX} \right)_i = U 2\pi R v_i \left(\frac{dR_V}{dX} \right)_i \quad (29)$$

where $A = \pi R^2$ is the cross-sectional area of the body (see Eq. (20)). Upon using the following definitions for the axial and radial velocities on the body surface (X, R) , respectively v_X and v_R , due to a source of strength q_i at point $(\xi_i, 0)$,

$$v_X = \frac{d}{dX} \left(\frac{q_i}{\sqrt{(X - \xi_i)^2 + R^2}} \right) \quad (30a)$$

and

$$v_R = \frac{d}{dR} \left(\frac{q_i}{\sqrt{(X - \xi_i)^2 + R^2}} \right), \quad (30b)$$

integrating the above expressions over the i th source segment and summing over the $N - 1$ source segments, the following two expressions for the resultant values of v_X and v_R on the body surface due to all the source segments, V_X and V_R , are obtained:

$$V_X(X, R) = \frac{U}{4\pi} \sum_{i=1}^{N-1} \left(\frac{dA}{dX} \right)_i \left[\frac{1}{\sqrt{(X - \xi_{Li})^2 + R^2}} - \frac{1}{\sqrt{(X - \xi_{Ri})^2 + R^2}} \right] \quad (31a)$$

and

$$V_R(X, R) = \frac{U}{4\pi R} \sum_{i=1}^{N-1} \left(\frac{dA}{dX} \right)_i \left[\frac{X - \xi_{Ri}}{\sqrt{(X - \xi_{Ri})^2 + R^2}} - \frac{X - \xi_{Li}}{\sqrt{(X - \xi_{Li})^2 + R^2}} \right] \quad (31b)$$

where ξ_{Li} and ξ_{Ri} , respectively the left and right ends of the i th line segment, are shown in Fig. 2.

Noting that V_X/U is a higher order quantity [42], the following consistent approximation for U_e on the body surface is obtained as

$$\begin{aligned} \frac{U_e}{U} &= \sqrt{\left[1 + \frac{V_X}{U} \right]^2 + \left[\frac{V_R}{U} \right]^2} = \sqrt{1 + 2 \frac{V_X}{U} + \frac{V_X^2}{U^2} + \frac{V_R^2}{U^2}} \\ &\approx 1 + \frac{V_X}{U} + \frac{1}{2} \frac{V_R^2}{U^2}. \end{aligned} \quad (32)$$

To correct the inaccuracies of the above slender-body theory at the ends of the body, a singularity gap correction proposed by Moran [43] is applied at the bow and stern ends. In this approach, the source distribution does not extend all the way to the end, but there is a gap equal in length to one half of the nose radius of the body. The gaps at the bow and stern ends, respectively γ_B and γ_S , then are approximated as

$$\gamma_B = \frac{R_{NO}}{2} = \frac{1}{4} \left(\frac{dR^2}{dX} \right)_{X=0} \approx \frac{R^2(X_2) - [R^2(X_1 = 0) = 0]}{4X_2} \quad (33a)$$

and

$$\gamma_S = \frac{R_{NL}}{2} = \frac{1}{4} \left(\frac{dR^2}{dX} \right)_{X=L} \approx \frac{R^2(X_N = L) - R^2(X_{N-1})}{4(X_N - X_{N-1})}, \quad (33b)$$

where R_{NO} and R_{NL} are respectively the nose radii at the bow and stern and R is the body radius.

A second modification is made to account for the effect of viscous flow on the stern pressure distribution. It is well-known that U_e does not approach zero at the stern end, as predicted by potential flow theory. The modification consists of an iterative procedure similar to that previously used by the author [44]. For the initial boundary layer calculation, the calculated values of U_e over the last 5% of the body are discarded and are replaced by a linear extrapolation of the calculated values for $X/L = 0.95$. The calculated displacement thickness δ^* is then added to the body, resulting in a somewhat larger body with a stern region which is significantly less blunt. For the second (and later) boundary layer calculations, the calculated U_e over the entire displacement body (up to the stern end, $X/L = 1.0$) is used. This is possible because of the much smoother variation of the shape of the stern region of the displacement body. The above procedure is repeated for a total of four iterations. In most cases, there is little difference in the calculated boundary layer characteristics between the third and fourth iterations, similar to the trend observed in Ref. 44. However, it is shown later that the method does not converge satisfactorily for a particular case of a ship with a blunt stern, thus giving an indication of the limit of applicability of the present procedure.

Computerized Calculation Procedure

The above calculations have been implemented in the form of a computer program called KBLST. The program first accepts input for the half-width f of the ship at a series of longitudinal x and vertical y stations. The input values of f may be from a data file, or (as is the case for most of the ships considered in this study) they may be analytically defined. The program then calculates the wetted area, the normal, and the source strength σ , given by Eqs. (15) and (17), for each ship panel defined by the input points. At each input x -station, the radii R_V and R_W in Eqs. (20) and (21) for the equal volume and equal wetted area bodies, respectively, are calculated. The edge velocity equations (Eqs. (27) to (33)) are calculated using the R_V body, while the boundary layer equations (Eqs. (22), (23), (25), and (26)) are calculated using either the R_V or R_W body, at the option of the user. If viscous flow effects are desired in the wave resistance calculations, the final calculated displacement thickness is added to the ship hull and revised values of the source strengths σ in Eqs. (15) and (17) are calculated. In many cases, the use of the R_V body to make the boundary layer calculations gives such a large displacement thickness that its addition to the original hull gives a resultant displacement hull which widens as the stern end is approached, i.e., gives source strengths in the stern region which are opposite in sign to those for the original hull. It was felt that this represented an unrealistically large modification. In these cases, σ is simply set equal to zero.

The wave resistance calculations are made using either slender-ship theory, Eqs. (15) and (16), or thin-ship theory, Eqs. (17) and (18). The principal part of these calculations is to obtain the amplitude spectrum as a function of longitudinal wave number $A^2(k_x)$ by using equations based on Eq. (16) in the slender-ship case and Eq. (18) in the thin-ship case. The wave resistance is then calculated by using an equation equivalent to Eq. (8). The program also contains the capability of calculating the wave elevation over a rectangular grid on the free surface by essentially taking the inverse Fourier transform of $A^2(k_x)$.

In summary, the program contains six options for calculating wave resistance for a given ship-Froude number case:

1. slender-ship—no displacement thickness,
2. slender-ship—displacement thickness using R_W body,
3. slender-ship—displacement thickness using R_V body,
4. thin-ship—no displacement thickness,
5. thin-ship—displacement thickness using R_W body,
6. thin-ship—displacement thickness using R_V body.

For most of the ship cases considered in the present study, all six options were exercised.

Due to the simplicity of the present calculation procedure, the program KBLST can be run with ease on a minicomputer such as the Hewlett-Packard 1000. Running time for the usual case of a ship with port and starboard symmetry, with one side modeled by approximately 200 to 300 panels, is typically 10 min for one of the above options. This makes it convenient to make parametric runs for the large number of ship forms described in the following chapter.

DESCRIPTION OF SHIP HULLS

Choice of Ship Hulls

The choice of ship hulls was based on a number of considerations. These included the availability of experimental data to validate the theoretical calculations, the existence of other thin- and slender-ship calculations to compare with the present approach, the need to cover a range of geometrical characteristics to illustrate the boundary layer effect, and the existence of analytic descriptions for hull shape which lead to convenient and precise input data.

Based on these considerations, four hulls were initially chosen, and a fifth was chosen after the start of the calculations: the Wigley hull [5], the Series 60 ($C_B = 0.60$) hull [5], the Sharma strut [45], the elliptic bow-parabolic stern (EP) strut ($B/L = 0.15$, where B = ship beam) suggested by Noblesse [46], and a thin EP (TEP) strut ($B/L = 0.05$). The Wigley and Series 60 hulls were obvious choices because extensive experimental and calculated data exist for these hulls. Both are among the test hulls suggested for the First and Second DTNSRDC (David Taylor Naval Ship Research and Development Center) Workshops on Ship Wave-Resistance Computations. The Sharma strut represents an extremely thin hull form for which a series of experimental data and calculations using thin-ship theory are given in Ref. 45. No experimental data exist for the EP and TEP struts. However, the EP strut is one of the suggested hull forms for calculation for the Second DTNSRDC Workshop and, as a result, a series of slender-ship calculations by Scragg [47] are available for comparison.

Due to the unsymmetrical fore and aft shapes of the EP strut, it was originally intended to make boundary calculations for this ship moving both forward and backward. These would show if the present calculation procedure could reproduce the general trend of the experimental results by Wigley [48] for a series of unsymmetrical ships towed both forward and backward. Unfortunately, the ends of this hull are too blunt for the present boundary layer calculation approach which is essentially applicable for slender-bodies. This was demonstrated by the fact that the boundary layer calculations did not converge. For example, there were usually large differences in the displacement thickness calculated for the third and fourth iterations.

Because of the above limitations, the TEP hull was added. The TEP hull is similar to the EP hull; the difference is that the width of the TEP is everywhere only 1/3 that of the EP. The boundary layer calculations converged for this new shape, and they were performed for the ship moving both forward (elliptic bow) and backward (parabolic bow).

Geometric Characteristics of Ship Hulls

Table 1 is a summary of the principal geometric characteristics of the hulls: length L , beam-to-length ratio B/L , beam-to-stern length ratio B/L_S , draft-to-length ratio H/L , block coefficient C_B , and wetted area coefficient C_S , where

- L is the length at the design waterline,
- B is the beam, the maximum width,
- L_S is the stern length, defined as the axial length from the stern end to the point where maximum width is initially attained,
- H is the draft,

Table 1 — Summary of Geometric Characteristics of the Five Chosen Hulls

Ship Hull	L (ft)	B/L	B/L_S	H/L	C_B	C_S
Wigley	20	0.0625	0.125	0.100	0.44	0.66
Series 60	20	0.133	0.266	0.053	0.60	0.71
Sharma	6.56	0.05	0.100	0.150	0.66	0.95
EP	20	0.15	0.600	0.075	0.86	0.95
TEP	20	0.05	0.200	0.075	0.86	0.96

$$C_B = \frac{V_D}{LBH} \text{ is the block coefficient,} \quad (34a)$$

$$C_S = \frac{S_W}{L(2H + B)} \text{ is the wetted area coefficient,} \quad (34b)$$

V_D is the volume of the underwater hull, and
 S_W is the wetted surface area.

Note that for all the hulls considered in the present study, the same definition for L_S applied to the bow area gives the bow length L_B equal to L_S , i.e.,

$$B/L_B = B/L_S. \quad (34c)$$

The table shows that the length L used in the calculations for the Wigley, Series 60, EP, and TEP hulls is 6.1 m (20 ft). This is representative of the length used in model tests of the Wigley and Series 60 hulls, and the unsymmetrical models towed in both the forward and reverse directions in Ref. 48. A length of 2 m (6.56 ft) is used for the Sharma strut, corresponding to that used in the model tests [45].

Table 2 gives the analytical formulas for the half-width f of the Wigley, Sharma, EP, and TEP hull forms. Figure 3 shows the stem and stern contours as well as the half-width section shapes at a series of longitudinal stations for the Series 60 hull form.

Figure 3 shows that the Series 60 hull has a nonvertical stern contour. (In the present study, the small deviations of the stem contour from the vertical are neglected.) The other four hulls, which are analytically defined, have vertical stem and stern contours. Table 2 and Fig. 3 show that the Sharma, EP, and TEP struts are wall-sided (no variation of half-width f with depth z) while the Wigley and Series 60 hulls have values of f which decrease with depth. This accounts for the low values of C_B and C_S for these two hulls. The Series 60 and EP hulls are significantly wider (larger values of B/L) than the other 3 hulls. The stern of the EP hull has a much larger value of B/L_S than the other four hulls and led to the previously mentioned difficulty in the boundary layer calculations. This in turn led to the necessity of adding the finer TEP hull, which has a stern whose value of B/L_S is comparable to those of the remaining hulls. The values of H/L range from the shallow draft value of 0.053 for the Wigley hull to 0.15 for the deeply submerged Sharma strut.

The Wigley and Sharma hulls are symmetrical fore and aft while the remaining three hulls are unsymmetrical. The EP and TEP hulls have a longitudinally parallel middle body section of constant width amounting to one-half of ship length. The remaining three hulls have widths which continually vary with x , with the maximum width occurring amidships.

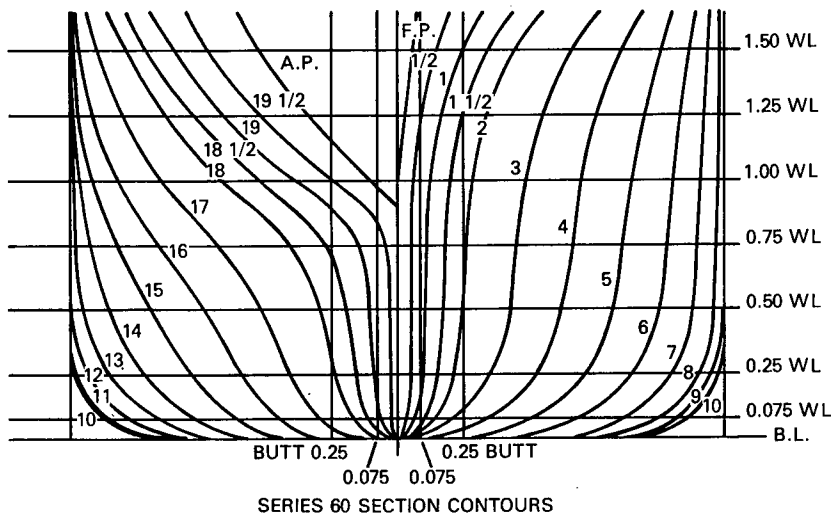
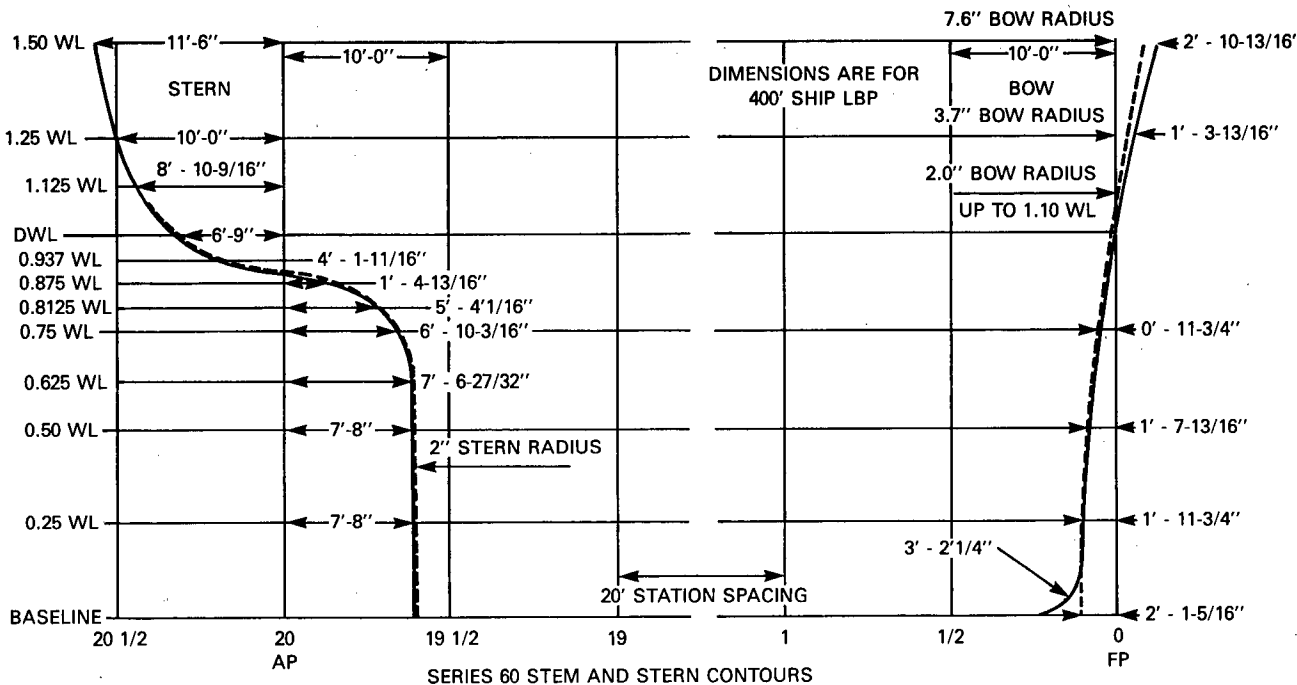


Fig. 3 — Geometric description of Series 60, $C_B = 0.60$ hull

Table 2 — Formulas for the Half-Width f of Four Ship Hulls

$x' = (x + L/2)/(L/2)$	
$x' = -1$ is the aft perpendicular	
$x' = +1$ is the forward perpendicular	
1. Wigley hull	
$f_1 = \frac{B}{2} (1 - x'^2) [1 - (z/H)^2]$	$-1 \leq x' \leq +1$
2. Sharma strut	
$f_2 = \frac{B}{2} (1 - x'^2)$	$-1 \leq x' \leq +1$
3. Elliptic bow-parabolic (EP) stern strut	
$f_3 = \frac{B}{2} [-4x'(1+x')]$	$-1 \leq x' \leq -\frac{1}{2}$
$f_3 = \frac{B}{2}$	$-\frac{1}{2} \leq x' \leq +\frac{1}{2}$
$f_3 = \frac{B}{2} \left[1 - 16 \left(\frac{1}{4} - \frac{x'}{2} \right)^2 \right]^{1/2}$	$+\frac{1}{2} \leq x' \leq +1$
4. Thin elliptic bow-parabolic (TEP) stern strut	
$f_4 = \frac{1}{3} f_3$	$-1 \leq x' \leq +1$

RESULTS

Matrix of Computer Runs

Table 3 summarizes information on the input data and type of computer runs made for each of the five hulls. The table gives:

- NX , the number of stations along the longitudinal x -axis at which the half-width f is input into the program,
- NZ , the number of stations along the vertical z -axis at which f is input,
- $Fn1$, the lowest Froude number Fn for which wave resistances are calculated,
- $Fn2$, the highest Froude number for which wave resistances are calculated,
- NF , the number of Fn cases for which wave resistances are calculated,
- NP , the number of calculations for each Fn case, neglecting boundary layer effects, and
- NV , the number of calculations for each Fn case, including boundary layer effects.

The value of NX for the three hulls which have continually varying widths along the x -axis (the Wigley, Series 60, and Sharma hulls) is 25, and it is respectively reduced to 22 and 17 for the EP and

Table 3 — Summary of Computer Runs
for the Five Ship Hulls

Ship Hull	NX	NZ	F_n1	F_n2	NF	NP	NV
Wigley	25	15	0.16	0.48	11	2	4
Series 60	25	7	0.14	0.36	18	2	4
Sharma	25	16	0.21	1.00	15	2	4
EP	22	16	0.15	1.00	16	2	0
TEP	17	16	0.15	1.00	16	2	8

TEP hulls which have parallel middle body sections extending over half the ship length. The value of NZ is 15 or 16 for the four hulls which are analytically defined (the Wigley, Sharma, EP, and TEP hulls). It is reduced to 7 for the Series 60, which corresponds to the number of vertical stations at which f is tabulated in Ref. 5. The Froude number range for the three hulls for which model test data are available (the Wigley, Series 60, and Sharma hulls) correspond to the experimental range. The Froude number range for the EP and TEP hulls approximates the range covered by the calculations of Scragg [47] for the EP strut.

Wave resistance calculations neglecting the boundary layer effect were made using both thin-ship and slender-ship theories for each Froude number for all five hulls. For the Wigley, Series 60, and Sharma hulls, four calculations including the boundary layer displacement thickness δ^* were also made for each Froude number: thin- and slender-ship theories, each using δ^* calculated for the R_V and R_W bodies, defined in Eqs. (20) and (21), respectively. Due to the previously mentioned nonconvergence of the boundary layer calculations, no wave resistance values accounting for the effect of δ^* are shown for the EP hull. On the other hand, eight such calculations were made for each Froude number for the TEP hull: the above-mentioned four calculations for the hull moving both forward (blunter elliptic bow, finer parabolic stern) and backward (finer parabolic bow, blunter elliptic stern).

Calculated Results

Figure 4 shows the variation of R_V and R_W , defined respectively in Eqs. (20) and (21), along the x -axis for the equivalent bodies of revolution which are used in the boundary layer calculations. In this figure, the R_W and R_V curves are represented by solid and dotted lines, respectively. Also, the R_V and R_W values for the Sharma strut are scaled up to the 20-ft ship length used for the other hulls, recalling that a 6.56-ft length is actually used for this hull (see Table 1).

Table 4 shows the ratio δ^*/δ_{FP}^* for the Wigley, Series 60, Sharma, and TEP hulls for five F_n cases, where δ^* is the displacement thickness for the R_V and R_W bodies at stern end, and δ_{FP}^* is the corresponding thickness for a flat plate of the same length and at the same velocity. For the TEP hull, the table shows this ratio for the hull moving both forward and backward.

Figure 5 shows the longitudinal variation of the ratio σ_D/σ_0 in the stern region for the hulls considered in Table 4 for $F_n = 0.35$, where σ_0 and σ_D are respectively the thin-ship values for source strength calculated for the original hull and the hull with displacement thickness added. As mentioned previously, if the displacement thickness modification is so large that it results in σ_D having a sign opposite to that of σ_0 , σ_D is simply set equal to zero. The present approach of using a body of revolution results in a constant value of δ^* being added to the hull at each longitudinal station. For the wall-sided Sharma and TEP struts, this results at a given x -station in a value of σ_D/σ_0 which does not vary with depth along the hull and is the value shown in Fig. 5. For the hulls which have half-widths which vary with depth, the Wigley and Series 60 hulls, the ratio σ_D/σ_0 also varies with depth. For these cases, the value shown in the figure represents an average over depth.

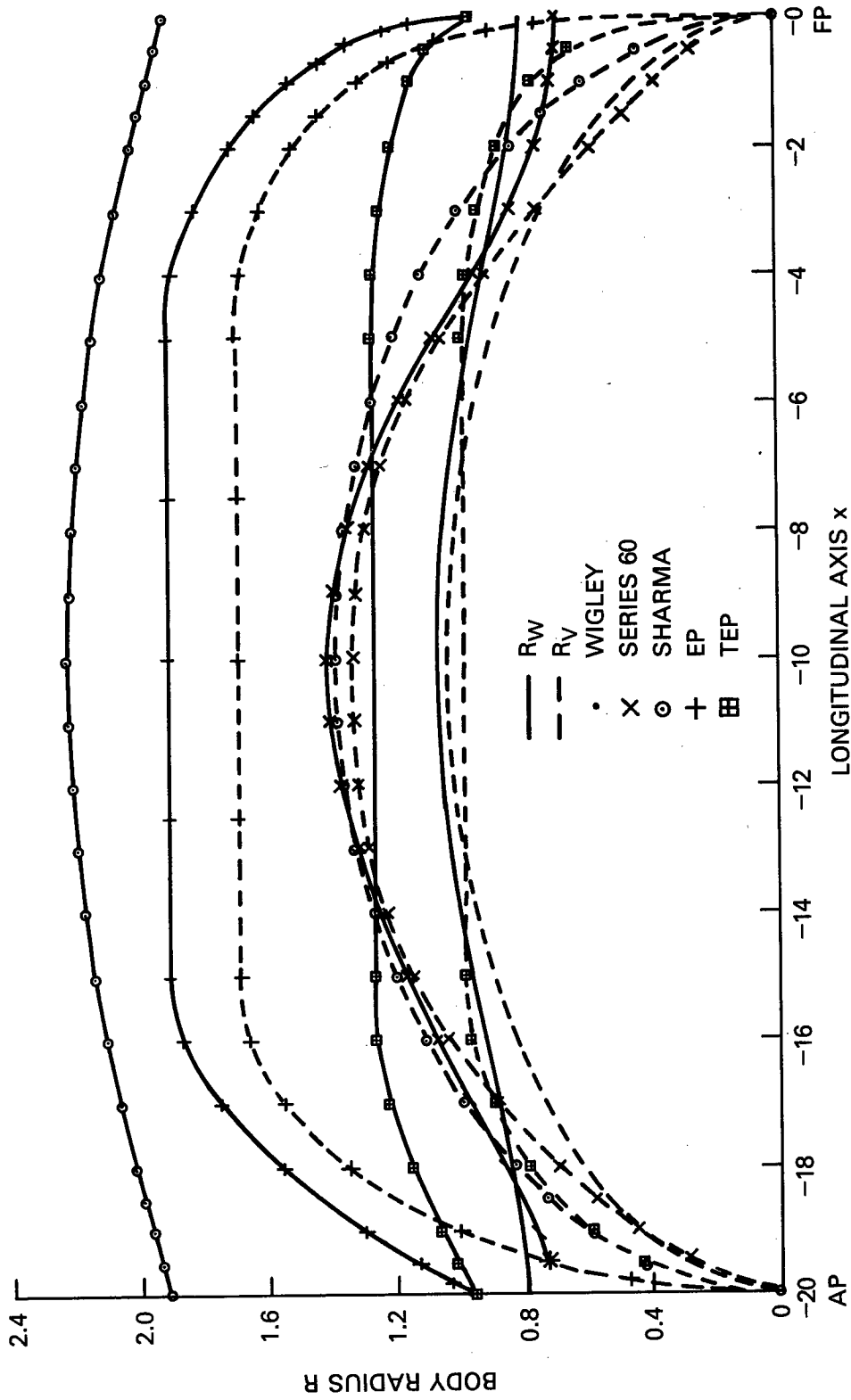


Fig. 4 -- Axisymmetric R_V and R_W bodies

Table 4 — Ratio δ^*/δ_{FP}^* at Stern End for Equal-Wetted Area (R_W) and Equal-Volume (R_V) Bodies of Revolution

	Wigley		Series 60		Sharma Strut	
	R_W	R_V	R_W	R_V	R_W	R_V
$Fn = 0.2$	1.17	5.29	3.38	8.33	1.44	5.64
$Fn = 0.35$	1.15	5.29	3.79	8.44	1.42	5.70
$Fn = 0.5$	1.14	5.27	—	—	1.40	5.74
$Fn = 0.7$	1.13	5.24	—	—	1.38	5.78
$Fn = 1.0$	1.12	5.22	—	—	1.36	5.81

	TEP Strut			
	Forward Elliptic Bow-Parabolic Stern		Backward Parabolic Bow-Elliptic Stern	
	R_W	R_V	R_W	R_V
$Fn = 0.2$	1.56	5.04	1.67	3.34
$Fn = 0.35$	1.54	5.05	1.66	3.36
$Fn = 0.5$	1.52	5.05	1.65	3.37
$Fn = 0.7$	1.50	5.05	1.64	3.37
$Fn = 1.0$	1.49	5.04	1.64	3.38

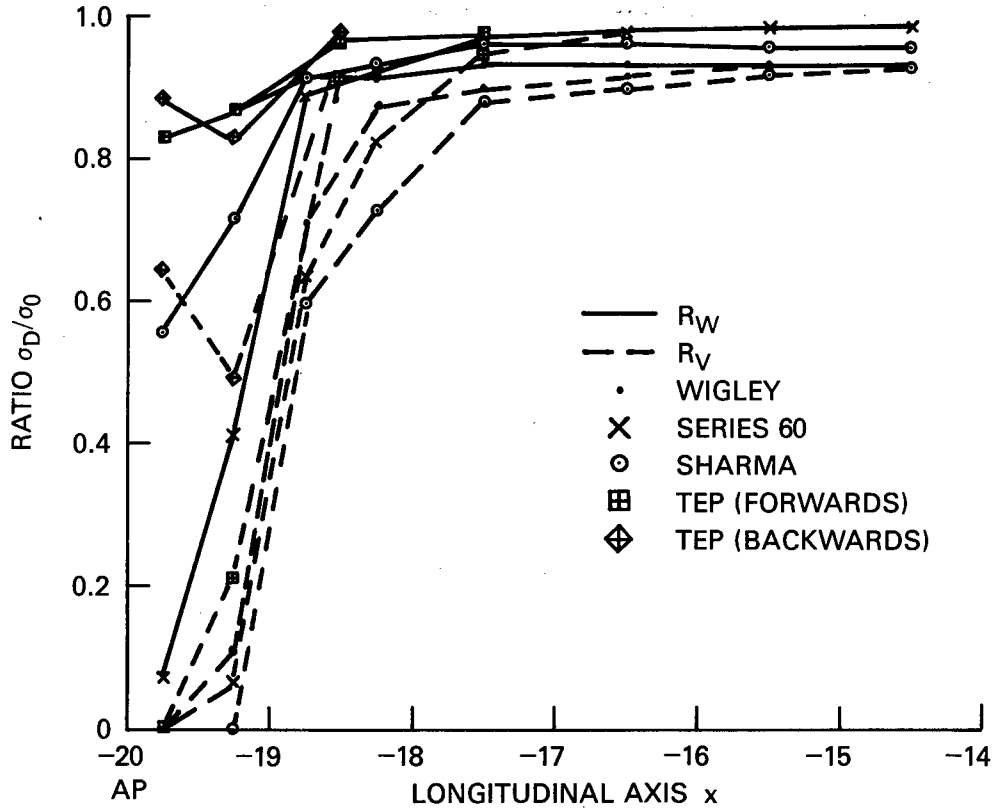


Fig. 5 — Variation of ratio of thin-ship source strengths with and without viscous modification σ_D/σ_0 in stern region

Figures 6, 7, 8, 9, and 10 show the calculated values of the wave resistance coefficient C_W as a function of F_n for the Wigley, Series 60, Sharma, EP, and TEP hulls, where C_W follows the definition used for both DTNSRDC Workshops on Wave Resistance:

$$C_W = \frac{D_W}{\frac{1}{2}\rho U^2 S_W} \quad (35)$$

The calculated results are also tabulated in Tables 5 to 9 for the above hulls. The notation for the calculated results in the figures is uniform and is as follows. Points plotted by the symbols \cdot , x , and $+$, denote, respectively, wave resistance values with no δ^* effect, δ^* using the R_W body, and δ^* using the R_V body. Values obtained by using slender-ship theory are enclosed by a circle, while those obtained by thin-ship theory are left uncircled. Most of the calculated results are shown in these figures. However, there are several exceptions. In the case of the thin Sharma strut, the slender- and thin-ship values (both with and without the δ^* effect) are so close that the slender-ship results have been omitted. Similarly, in the case of the Series 60 hull for $F_n \leq 0.25$, the thin- and slender-ship results, for cases where the δ^* effect is included, are sufficiently close that the slender-ship results have again been omitted. In these cases, the reader is referred to the corresponding tables for a more detailed look at the calculated C_W values.

Figures 6, 7, and 8 show experimental data for the Wigley, Series 60, and Sharma hulls. A range of data from a number of experiments are shown for the Wigley and Series 60 hulls, while the data from the single series of experiments reported in Ref. 45 are shown for the Sharma strut. The majority of the experimental data for the Wigley and Series 60 hulls reported in Ref. 5 are for the case where the ship model is free to sink and trim. This refers to the fact that the draft and pitch angle (rotation about the y axis) of the ship hull moving at forward speed are generally different from those for the ship at rest. These changes in draft (sinkage) and pitch (trim) arise due to the perturbation flow field induced by the motion of the ship. The numerical results of Dawson, Gadd, and others, reported in Ref. 5, indicate that the effect of sinkage and trim is to increase the wave resistance values as compared to those for a fixed model. Since the present calculations are made for a fixed model, it is desirable to convert the experimental data to this case. Fortunately, Chen and Noblesse [49] have performed this conversion for the Wigley hull, using as a guide the reduction factors given in the previously mentioned numerical results [5]. Thus, the experimental range shown in Fig. 6 is taken from Ref. 49 and applies for the fixed model case. Figure 6 also shows, as discrete points, the recent experimental results of Kajitani et al. [50] specifically for a fixed model.

The experimental range shown for the Series 60 in Fig. 7 is taken from Ref. 5, and the results are largely for cases where the model is free to sink and/or trim. Only the lowest set of data is for the fixed model case. Finally, the experiments for the Sharma strut [45] are for the fixed model case.

Figures 6 to 9 also show calculations of other authors using similar thin-ship and slender-ship calculations to compare with the present calculations. Figure 6 shows thin- and slender-ship calculations by Lackenby, on p. 345 of Ref. 5, for the Wigley hull. Figures 7 and 9 show slender-ship calculations by Scragg [47] for the Series 60 and EP hulls. Figure 8 shows thin-ship calculations [45] for the Sharma strut. In all of these calculations, the effect of viscosity has been neglected.

Figure 11 shows the differences ΔC_W between the calculated values of C_W for the TEP hull in forward (finer parabolic stern) and backward (blunter elliptic stern) motions

$$\Delta C_W = C_{WF} - C_{WB} \quad (36)$$

where C_{WF} and C_{WB} are respectively the values of C_W for forward and backward motions. The results are shown for thin- and slender-ship theories for viscous modifications using both the R_W and R_V bodies. Table 10 shows these differences in tabulated form.

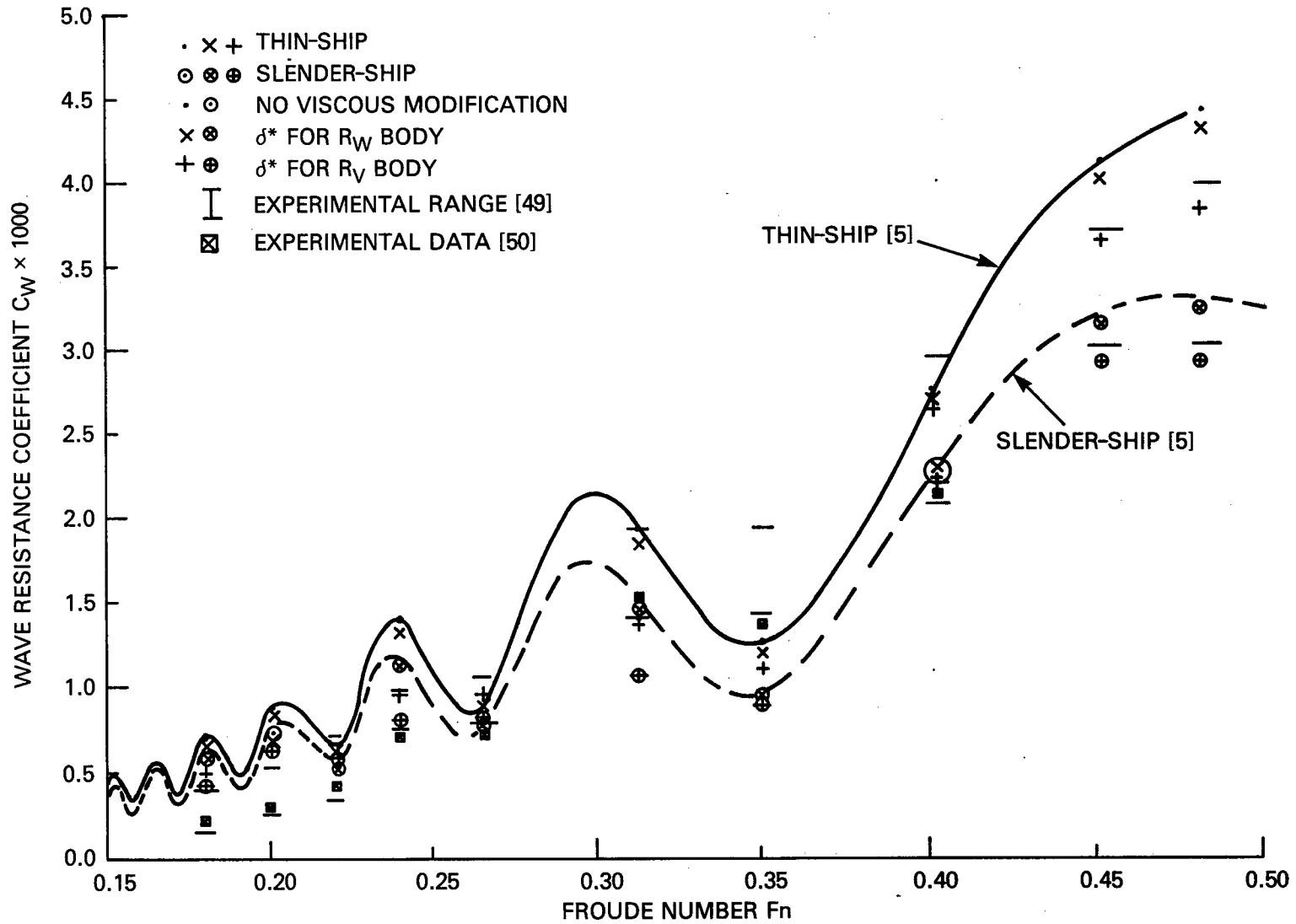


Fig. 6 - Wave resistance coefficients for Wigley hull

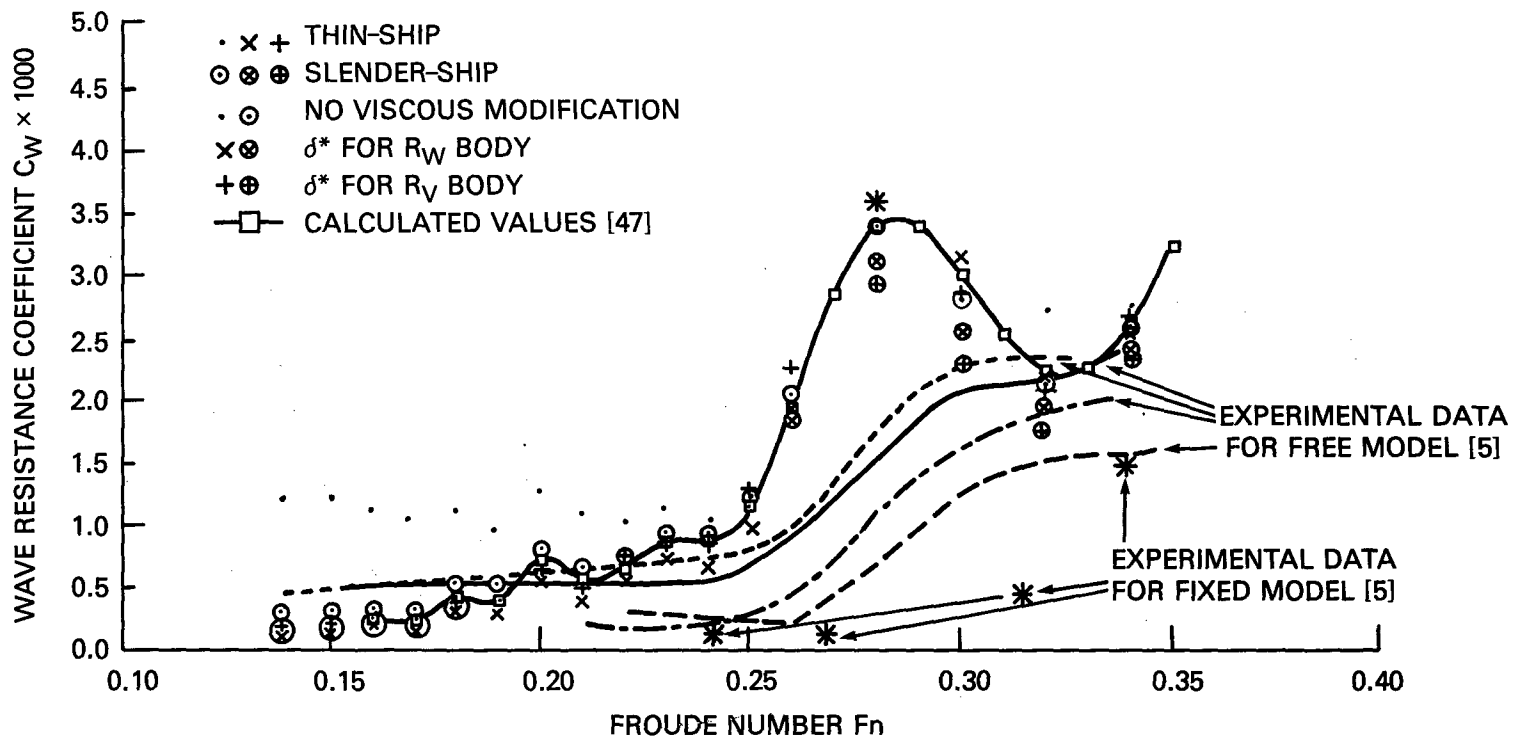


Fig. 7 — Wave resistance coefficients for Series 60, $C_B = 0.60$ hull

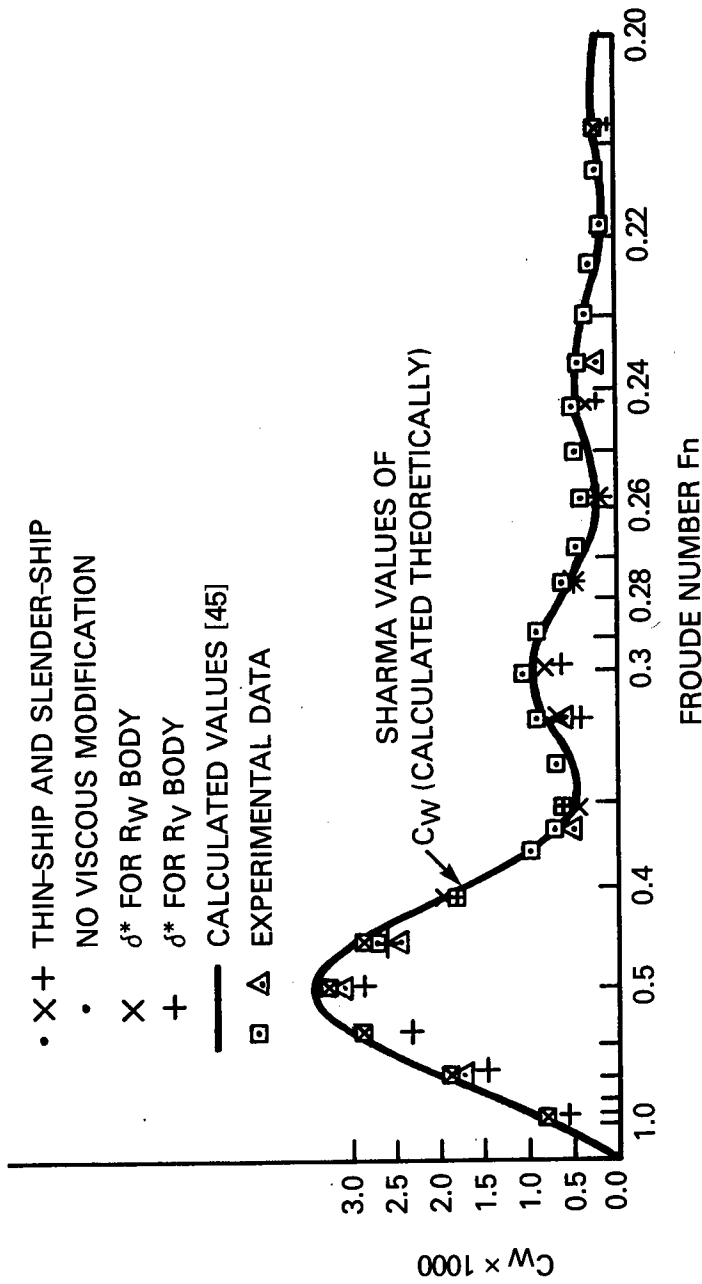


Fig. 8 — Wave resistance coefficients for Sharma strut

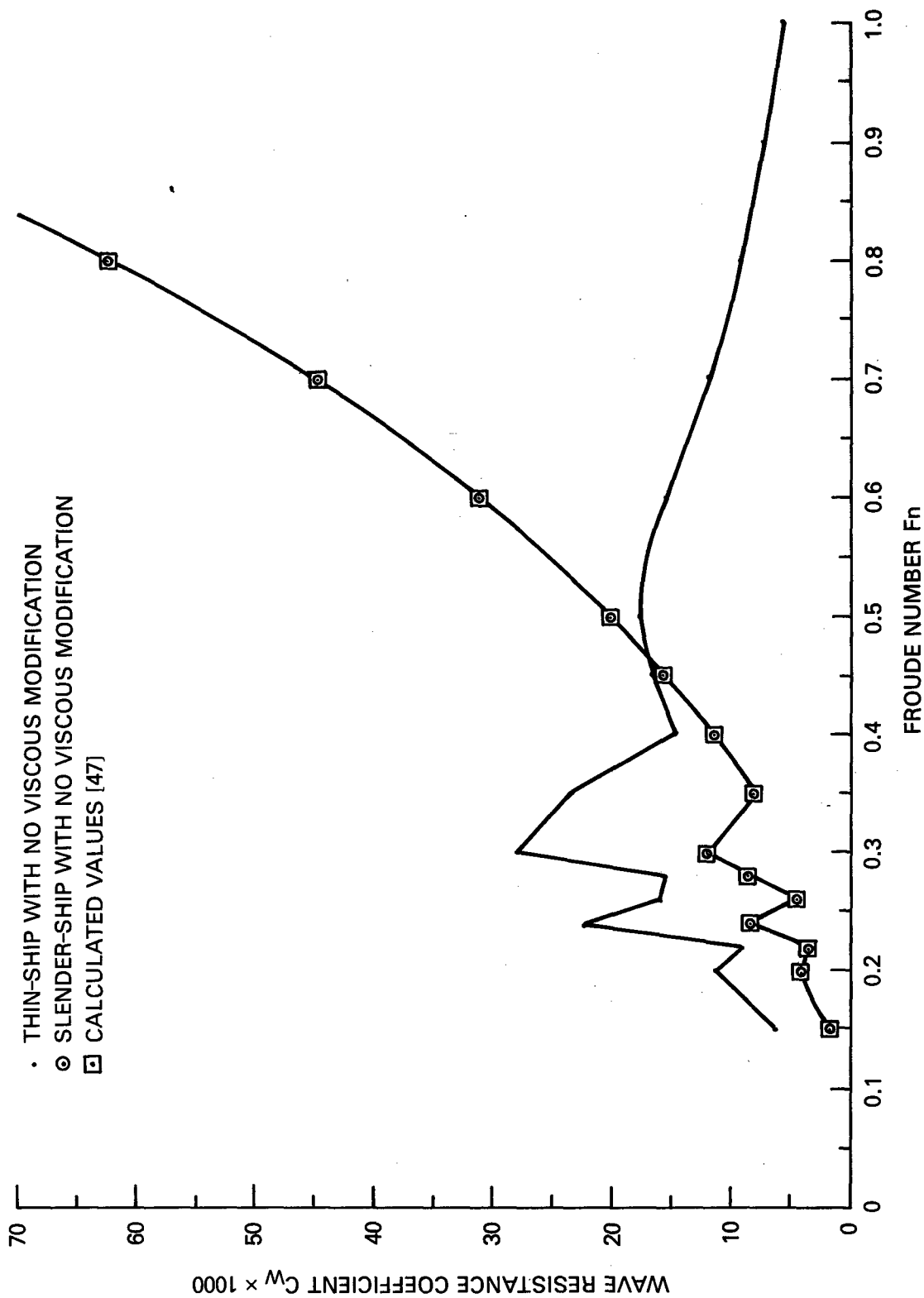


Fig. 9 — Wave resistance coefficients for EP strut

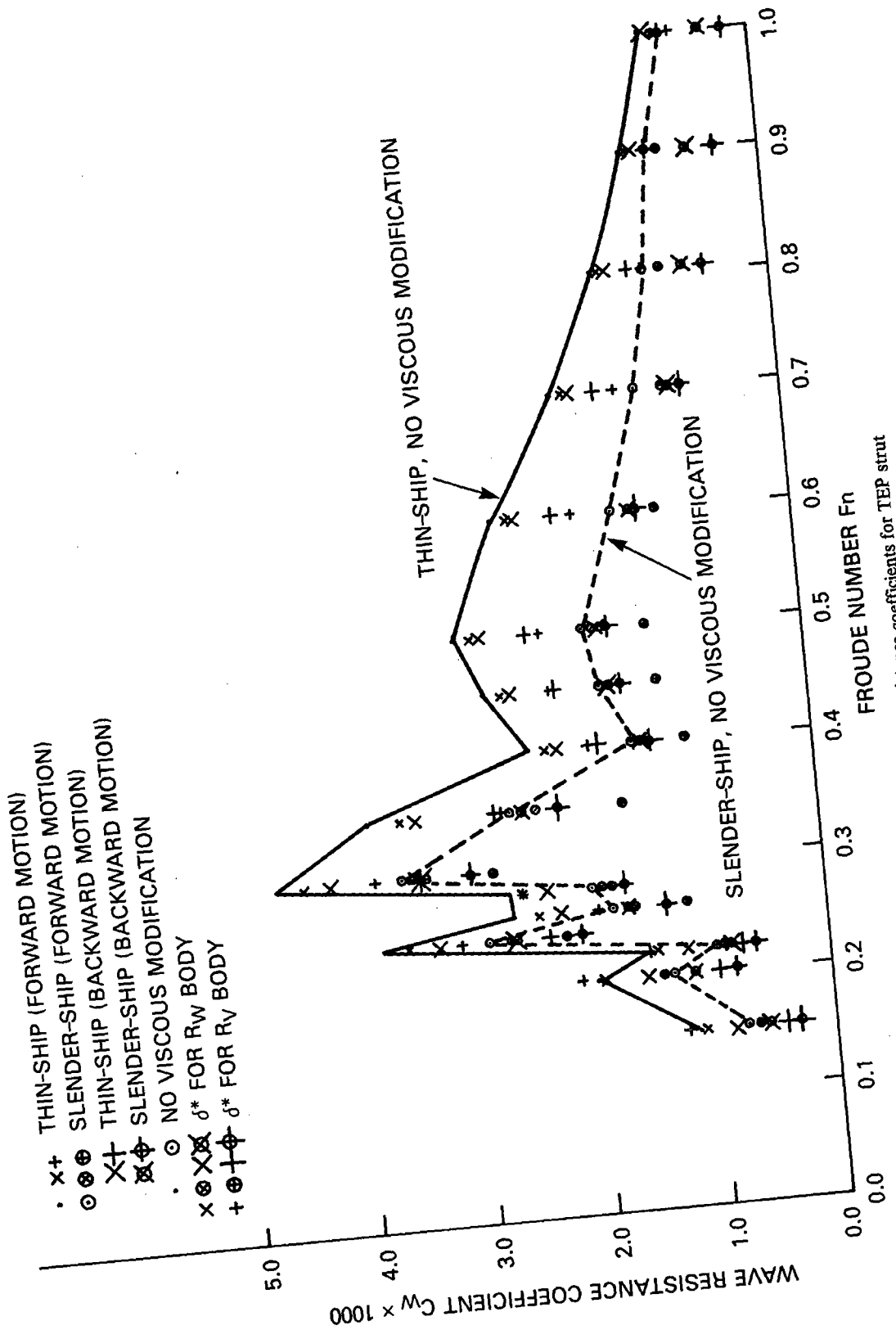


Fig. 10 — Wave resistance coefficients for TEP strut

Table 5 — Calculated Values of $C_W \times 1000$ for Wigley Hull

F_n	$\delta^* = 0$		δ^* for R_W Body		δ^* for R_V Body	
	Thin Ship	Slender Ship	Thin Ship	Slender Ship	Thin Ship	Slender Ship
0.160	0.334	0.303	0.305	0.284	0.374	0.332
0.180	0.701	0.626	0.652	0.584	0.493	0.433
0.199	0.855	0.755	0.820	0.725	0.728	0.635
0.219	0.636	0.553	0.614	0.536	0.678	0.585
0.239	1.375	1.170	1.317	1.124	0.948	0.799
0.265	0.913	0.772	0.887	0.752	0.946	0.799
0.312	1.917	1.497	1.849	1.447	1.357	1.059
0.349	1.229	0.963	1.195	0.939	1.102	0.894
0.401	2.750	2.286	2.688	2.236	2.652	2.219
0.451	4.139	3.242	4.033	3.164	3.673	2.915
0.481	4.445	3.331	4.331	3.253	3.842	2.930

Table 6 — Calculated Values of $C_W \times 1000$ for Series 60, $C_B = 0.60$ Hull

F_n	$\delta^* = 0$		δ^* for R_W Body		δ^* for R_V Body	
	Thin Ship	Slender Ship	Thin Ship	Slender Ship	Thin Ship	Slender Ship
0.14	1.221	0.262	0.114	0.136	0.162	0.137
0.15	1.216	0.304	0.134	0.163	0.180	0.161
0.16	1.100	0.316	0.173	0.223	0.273	0.253
0.17	1.048	0.286	0.142	0.199	0.267	0.257
0.18	1.135	0.491	0.295	0.356	0.373	0.348
0.19	0.954	0.479	0.316	0.402	0.494	0.465
0.20	1.267	0.801	0.560	0.627	0.634	0.592
0.21	1.091	0.620	0.383	0.446	0.473	0.430
0.22	1.017	0.721	0.555	0.624	0.748	0.683
0.23	1.169	0.926	0.719	0.805	0.869	0.828
0.24	1.046	0.927	0.657	0.801	0.837	0.829
0.25	1.148	1.217	0.984	1.113	1.295	1.203
0.26	1.987	2.044	1.955	1.908	2.308	1.999
0.28	4.036	3.398	3.625	3.095	3.637	2.954
0.30	3.898	2.904	3.162	2.589	2.932	2.322
0.32	2.759	2.163	2.223	1.951	2.147	1.789
0.34	2.779	2.602	2.578	2.436	2.713	2.397
0.36	4.260	4.020	4.203	3.847	4.417	3.841

MULTIPLY BY 1000

Table 7 — Calculated Values of $C_W \times 1000$ for Sharma Strut

F_n	$\delta^* = 0$		δ^* for R_W Body		δ^* for R_V Body	
	Thin Ship	Slender Ship	Thin Ship	Slender Ship	Thin Ship	Slender Ship
0.208	0.208	0.204	0.145	0.142	0.092	0.090
0.219	0.137	0.135	0.127	0.124	0.170	0.166
0.229	0.317	0.307	0.294	0.288	0.287	0.280
0.243	0.405	0.396	0.320	0.313	0.213	0.207
0.258	0.225	0.221	0.193	0.189	0.207	0.201
0.276	0.524	0.514	0.519	0.509	0.532	0.521
0.301	0.922	0.900	0.810	0.791	0.589	0.573
0.334	0.501	0.488	0.428	0.417	0.335	0.325
0.365	0.667	0.659	0.677	0.667	0.760	0.747
0.408	1.953	1.922	1.920	1.888	1.857	1.823
0.447	2.937	2.873	2.814	2.753	2.505	2.448
0.500	3.382	3.282	3.193	3.101	2.700	2.614
0.578	3.022	2.890	2.833	2.713	2.318	2.216
0.709	2.038	1.883	1.910	1.767	1.541	1.421
1.000	0.875	0.705	0.823	0.666	0.661	0.532

Table 8 — Calculated Values of $C_W \times 1000$ for (Elliptic Bow-Parabolic Stern) EP Strut

F_n	$\delta^* = 0$	
	Thin Ship	Slender Ship
0.15	6.61	1.42
0.20	11.20	3.95
0.22	8.97	3.29
0.24	22.30	8.26
0.26	15.97	4.41
0.28	15.58	8.46
0.30	27.68	11.93
0.35	23.16	7.86
0.40	14.45	11.29
0.45	16.47	15.57
0.50	17.87	19.75
0.60	15.41	30.95
0.70	11.79	44.64
0.80	9.12	62.34
0.90	7.06	86.62
1.00	5.57	115.06

Table 9 — Calculated Values of $C_w \times 1000$ for (Thin Elliptic Bow-Parabolic Stern) TEP Strut in Forward (Parabolic Stern) and Backward (Elliptic Stern) Motion

F_n	$\delta^* = 0$		Forward Motion				Backward Motion			
			$\delta^*(R_w)$		$\delta^*(R_v)$		$\delta^*(R_w)$		$\delta^*(R_v)$	
	TS	SS	TS	SS	TS	SS	TS	SS	TS	SS
0.15	1.14	0.70	1.10	0.66	1.24	0.74	0.83	0.55	0.39	0.29
0.20	1.96	1.35	1.91	1.30	2.11	1.42	1.55	1.17	0.94	0.81
0.22	1.52	0.95	1.45	0.89	1.52	0.95	1.20	0.84	0.74	0.62
0.24	3.77	2.87	3.57	2.69	3.11	2.22	3.26	2.65	2.36	2.11
0.26	2.64	1.80	2.44	1.62	1.93	1.17	2.25	1.67	1.59	1.34
0.28	2.64	1.95	2.55	1.86	2.55	1.79	2.35	1.87	1.91	1.68
0.30	4.63	3.58	4.41	3.38	3.81	2.79	4.19	3.42	3.40	3.00
0.35	3.81	2.59	3.55	2.39	2.68	1.65	3.42	2.50	2.73	2.20
0.40	2.39	1.50	2.26	1.41	1.90	1.07	2.18	1.46	1.82	1.36
0.45	2.72	1.74	2.60	1.66	2.15	1.27	2.53	1.68	2.14	1.59
0.50	2.94	1.84	2.82	1.77	2.23	1.32	2.75	1.73	2.33	1.66
0.60	2.53	1.52	2.42	1.49	1.86	1.14	2.37	1.31	2.02	1.26
0.70	1.93	1.22	1.85	1.21	1.41	0.98	1.82	0.94	1.56	0.84
0.80	1.49	1.04	1.44	1.06	1.10	0.93	1.41	0.72	1.21	0.56
0.90	1.16	0.95	1.11	0.96	0.84	0.86	1.09	0.60	0.94	0.37
1.00	0.91	0.75	0.88	0.80	0.67	0.81	0.87	0.41	0.75	0.20

Table 10 — Differences in Calculated Values of $C_w \times 1000$ for TEP Strut in Forward Motion Minus Corresponding Value in Backward Motion

F_n	δ^* for R_w Body		δ^* for R_v Body	
	Thin Ship	Slender Ship	Thin Ship	Slender Ship
0.15	0.27	0.11	0.85	0.45
0.20	0.36	0.13	1.17	0.61
0.22	0.25	0.05	0.78	0.33
0.24	0.31	0.04	0.75	0.11
0.26	0.19	-0.05	0.34	-0.17
0.28	0.20	-0.01	0.64	0.11
0.30	0.22	-0.04	0.41	-0.21
0.35	0.13	-0.11	-0.05	-0.55
0.40	0.08	-0.05	0.08	-0.29
0.45	0.07	-0.02	0.01	-0.32
0.50	0.07	0.04	-0.10	-0.34
0.60	0.05	0.18	-0.16	-0.12
0.70	0.03	0.27	-0.15	0.14
0.80	0.03	0.34	-0.11	0.37
0.90	0.02	0.36	-0.10	0.49
1.00	0.01	0.39	-0.08	0.61

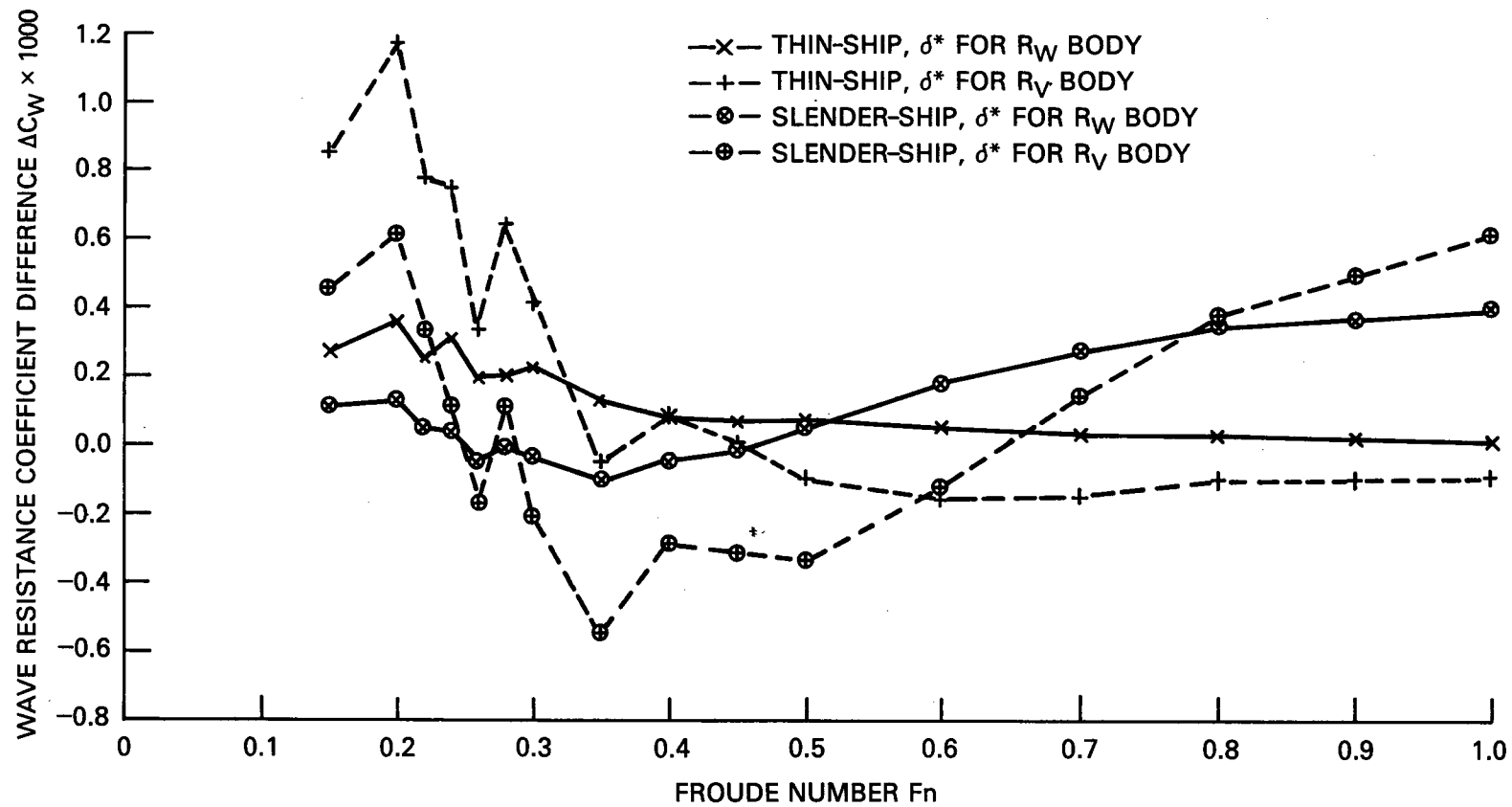


Fig. 11 — Differences in wave resistance coefficient between forward and backward motions for TEP strut

DISCUSSION OF RESULTS

The shapes of the equivalent bodies of revolution are discussed first. The source strength modifications resulting from the boundary layer calculations using these bodies are discussed next. The wave resistance calculations, in terms of their comparison with other theoretical values as well as with experimental data, are discussed for each individual hull. Finally, some overall trends are indicated.

Equivalent Bodies of Revolution

Figure 4 shows that for all five hulls, the equal-wetted area (R_W) body has a larger radius than the corresponding equal-volume (R_V) body. With the exception of the stern end of the Series 60 hull, the difference between the two bodies is largest at both ends, with R_V approaching 0 and $|(1/R_V)dR_V/dX| \gg |(1/R_W)dR_W/dX|$. This leads to the previously noted, larger streamline convergence effect (see Eq. (22)) for the R_V body.

The exception at the stern end in the case of the Series 60 hull is simply due to its nonvertical stern contour (shown in Fig. 3) effectively resulting in the ship having zero draft at the stern end. According to Eq. (24b), R_W in this case is also 0.

The asymmetry of the EP and TEP is clearly shown by the fact that $|dR/dx|$ for both the R_V and R_W bodies is larger at the elliptic bow end.

Boundary Layer Modification to Source Strength

Table 4 shows that, with the exception of the Series 60 hull, the use of the R_W body leads to values δ^* which are only 1.1 to 1.7 times the corresponding values for a flat plate. On the other hand, the use of the R_V body gives values of δ^* which are 3.4 to 8.4 times the flat plate values. This is largely due to the previously mentioned larger streamline convergence effect for the R_V body. In the case of the Series 60 hull, which has a nonvertical stern contour resulting in $R_W = 0$ at the stern end, δ^* for the R_W body is 3.8 times the flat plate value. The above results show that the streamline convergence term tends to dominate the growth of the boundary layer in the stern region. Since it has previously been shown that the R_W and R_V bodies tend to bracket the actual streamline convergence effect, the values of δ^* calculated on these two bodies may also tend to bracket the actual value of δ^* . The table also shows that over a fivefold change in Froude number, which (for a given model length) is equivalent to a fivefold change in Reynolds number, there is little change in the ratio δ^*/δ^*_{FP} .

Figure 5 shows the ratio σ_D/σ_0 of the modified and original values of source strength in the stern region of the hulls. In accordance with the previously noted fact that δ^* for the R_W body is always less than the corresponding value for the R_V body, the ratio σ_D/σ_0 using δ^* for the R_V body, at a given value of x , is always less than that for the R_W case. With the exception of the case for the TEP hull moving backward, the values of the ratio for the R_V case all reach zero within 1 ft of the stern end. On the other hand, none of the values of σ_D/σ_0 reach zero for the R_W case. The minimum value in the case of the Series 60 hull, which has a nonvertical stern contour and $R_W = 0$ at the stern end, is approximately 0.1. For the other hulls, the minimum value ranges between 0.55 and 0.90.

Again, with the exception of the TEP hull moving backward, the ratio increases with increasing distance from the stern end. At $x = -16$, which corresponds to 20% of L away from the stern end, all the values of σ_D/σ_0 are greater than 0.9, i.e., within 0.1 of 1.0, which is the value corresponding to no modification due to δ^* . This is to be expected because δ^* is largest at the stern end and decreases away from the stern.

The anomalies in the case of the TEP hull moving backward may be largely explained by the bluntness of the elliptic end, as shown in Fig. 4, and the thin-ship definition of σ given by Eq. (17).

Figure 4 shows that the elliptic end of TEP (in the region near $x = 0$) is clearly the second bluntest end (to the EP elliptic end which failed to converge in the boundary layer calculations) in both the R_V and R_W cases. The figure indicates that in this blunt region the displacement thickness (which is added normal to the hull surface) is largely in the x direction, with a relatively small contribution to the thickness f . Equation (17) shows that the resulting value of σ_D would be relatively close to σ_0 , giving the anomalous increase in σ_D/σ_0 at the stern end. This is one indication of the inapplicability of thin-ship theory for blunt ends.

The behavior of σ_D/σ_0 in the stern region may be compared with the constant reduction factor of 0.6 for the entire stern used by Havelock [18]. If one considers the region nearest the stern end (where most of the change in hull geometry takes place) as most significant and takes the point 5% of L away from the stern end as being representative, Fig. 5 shows that values for the R_V case are clustered around 0.4 while those for the R_W case range from 0.65 to 0.9. These values tend to bracket the factor assumed in Ref. 18.

Wigley Hull

Figure 6 shows values of wave resistance coefficients calculated by the present approach, the theoretical results by Lackenby as reported in Ref. 5, the range of experimental data corrected for sinkage and trim [49], and the recent measured data [50] specifically for a fixed model.

Perhaps the most noticeable feature of the figure is the striking agreement between the thin-ship and slender-ship results, neglecting viscous effects, of the present approach and those of Lackenby. The agreement is usually to within plotting accuracy. This agreement confirms the correctness of the numerical part of the present potential flow approaches.

Without viscous flow effects, the thin-ship values are always higher than corresponding slender-ship values. Similarly, for a given boundary layer approach using either the R_W or R_V body the thin-ship values are again higher than those using slender-ship theory.

As in previous studies, the effect of the boundary layer is usually to reduce the value of C_W . For both slender- and thin-ship theories, the reduction is larger for the approach using the R_V body than for the R_W body. This is due to the larger values of δ^* for the R_V body. For a given ship theory, the difference in C_W between the two boundary layer approaches ranges from nearly zero at certain Fn to 0.4×10^{-3} at other Fn . The reduction for the approach using the R_W body is always quite small.

For $Fn < 0.2$, all the calculated values lie above the experimental range. For $Fn > 0.2$, considering the C_W values for both the R_V and R_W bodies, the calculated values for thin-ship theory tend to either lie within the experimental range or bracket the upper limit. The calculated values for slender-ship theory tend to either lie within the experimental range or bracket the lower limit. The recent experimental data specifically for a fixed model [50] consistently fall near the lower limit of the experimental range [49]. Noting that the results in Ref. 49 are obtained by applying correction factors to data originally obtained for models free to sink and trim, the data in Ref. 50 tend to indicate that the lower range of the experimental data in Ref. 49 may be more appropriate for a fixed model.

On the whole, the trend of the viscous correction is encouraging. If the boundary layer calculations for the R_W and R_V bodies are viewed as bracketing the actual viscous flow effect, the results indicate that a more accurate boundary layer modeling will bring the thin-ship calculations into closer agreement with experimental data and the slender-ship calculations into rather good agreement for most Fn cases.

Series 60 Hull

Figure 7 shows the values of C_W calculated by the present approach, by Scragg [47] using a similar slender-ship approach, and the range of experimental data in Ref. 5. These values are for a model free to sink and trim except for the fixed model case indicated by the four discrete points in the lower right-hand corner.

The slender-ship values of C_W , without viscous effects, for the present approach are in reasonably good, but not precise, agreement with those of Ref. 47. Quadrilateral panels are used in the present approach while triangular panels are used in Ref. 47. It will be shown later in the case of the EP hull where quadrilateral panels are used in both approaches that the agreement is to within plotting accuracy.

As in the case of the Wigley hull in the absence of viscous effects, the thin-ship values are usually higher than corresponding slender-ship values. When viscous effects are included, some trends are the same as those for the Wigley hull while others are not. Figure 7 and Table 6 show that the effect of adding δ^* to the hull is again to generally (but not always) reduce the value of C_W . Unlike the Wigley hull case, the reduction due to δ^* calculated for the R_W body may be large and often slightly exceeds the reduction for the R_V case. This is due to the previously mentioned fact that R_W also goes to zero at the stern end for this hull, which has a nonvertical stern contour. In the R_V case, the thin-ship values are higher than the slender-ship values, as in the case when viscous effects are neglected. On the other hand, in the R_W case the slender-ship values are higher for $Fn \leq 0.25$.

The agreement of the calculated results with experimental data is considerably worse than for the Wigley hull. Even with the boundary layer correction, the thin-ship results for $Fn \geq 0.25$ generally lie well above the upper limit of the experimental data. In this Froude number range, the slender-ship results (with the δ^* correction) are lower than the thin-ship results. At times they lie within the experimental range for the free model case but are considerably higher than the data for the fixed model case. For the lower Fn , most of the calculated data, with the notable exception of the potential flow thin-ship results, lie within the range of the experimental data but again appear to be higher than the extrapolation of the fixed model data. It appears that for this full hull form ($B/L = 0.13$) with a flat bottom, a more complex ship theory is required. The results shown in Ref. 5 indicate that the use of low speed theory, such as that by Dawson [8], or Guilloton's method [11,12] may give substantially more accurate results.

Sharma Strut

As mentioned previously, the slender-ship results are not plotted in Fig. 8 due to their closeness to the thin-ship results. This is not surprising because of the fineness of the hull ($B/L = 0.05$). Table 7 shows that in all cases, with and without the boundary layer modification, the values of C_W calculated by thin-ship theory are slightly higher than the corresponding slender-ship values. This is in accordance with the trend previously noted for the Wigley and Series 60 hulls. Also, as in the Wigley case, the thin-ship results (with no δ^* effect) calculated by the present approach are in excellent agreement with corresponding results by Sharma [45].

As in the case of the previous two hulls, the effect of adding δ^* is to reduce the value of C_W . In the case of the Wigley hull, the reduction is generally small for the R_W case and of variable size (dependent on Froude number) for the R_V case. The calculated values with no δ^* effect are already in reasonably good agreement with experimental results, and the addition of the small reduction for the R_W case improves the agreement at the high Fn range. The use of δ^* for the R_V case generally worsens the agreement. This is probably because for this deeply submerged hull ($H/L = 0.15$) the use of two-dimensional boundary layer theory, instead of the present axisymmetric approach, may be more appropriate over most of the hull. In the two-dimensional approach, where the streamlines are assumed not to change in the z -direction, the streamline convergence term in Eq. (22) goes to zero. This is the effect which is emphasized more by use of the R_V body than the R_W body.

EP Strut (Elliptic Bow-Parabolic Stern, $B/L = 0.15$)

Figure 9 shows the thin-ship and slender-ship values calculated by the present approach and the slender-ship calculations using a similar theory by Scragg [47]. As mentioned previously, the boundary layer calculations for this hull failed to converge due to the extremely blunt stern, $B/L_S = 0.60$.

The figure shows that, except for the cross-over region of $0.4 \leq Fn \leq 0.5$, there are usually large differences between the thin-ship and slender-ship values. This is not surprising because of the fullness of the entire hull, $B/L = 0.15$ and the bluntness of the bow and stern, both of which have $B/L = 0.6$. Unlike the other hulls, the slender-ship results are not generally lower than the thin-ship values. They are substantially higher for $Fn \geq 0.5$.

The slender ship values of Ref. 47 agree to within plotting accuracy with the present results. This is not surprising because the similarity of the approaches and the use of quadrilateral panels in both studies. This contrasts with the previous Series 60 case, where the use of triangular panels in Ref. 47 leads to small, but noticeable, differences between the two approaches.

TEP Strut (Thin Elliptic Bow-Parabolic Stern, $B/L = 0.05$)

Figure 10 shows the thin- and slender-ship values calculated by the present approach, with and without viscous effects, for the ship moving both forward (finer parabolic stern) and backward (blunter elliptic stern). Figure 11 shows the difference ΔC_W , C_W for forward motion minus C_W for backward motion, for thin- and slender-ship theories using δ^* calculated for the R_V and R_W bodies.

Note that, without viscous effects, the present thin- and slender-ship theories should give the same value of C_W for both forward and backward motions. This was confirmed by several computer runs. Noblesse [51] points out that this need not be the case in higher order slender-ship theories.

Many of the trends shown in Fig. 10 are similar to those for the Wigley hull. Without viscous effects, the thin-ship values are always higher than the corresponding slender-ship values. Similarly, for a given direction of motion and a given δ^* approach, the thin-ship values are always higher. As before, the reduction in C_W for the R_W case using thin-ship theory is small for forward motion. However, the reduction is somewhat larger for backward motion (blunt stern) in certain Fn cases, for both thin- and slender-ship theories. This is because δ^*/δ_{FP}^* for the R_W case for the Wigley hull is only 1.2, and increases to 1.6-1.7 for the TEP hull.

As mentioned previously, one of the major points of interest for this unsymmetrical hull is to see if the present calculation procedure can reproduce the experimental trend for ΔC_W obtained by Wigley [48] for several unsymmetrical hulls towed in both directions. The general experimental trend is for C_W to be larger for the finer stern, i.e., $\Delta C_W > 0$ in the range $0.2 \leq Fn \leq 0.5$, with ΔC_W reaching a maximum at $Fn \approx 0.3$. For $Fn > 0.5$, the experimental results show little difference in the value of C_W in either direction of motion, i.e., $\Delta C_W \approx 0$.

Figure 11 shows that this trend is reproduced quite well by the thin-ship approach using δ^* calculated for the R_W body and approximately for the R_V body. Unfortunately, the experimental trend is not reproduced by the slender-ship results. For a given approach, the slender-ship curve is approximately parallel to, but below, the corresponding thin-ship curve for $Fn < 0.40$. This often results in C_W having the incorrect sign. For $Fn > 0.5$, the slender-ship curve increases to large positive values instead of approaching the nearly zero values obtained experimentally. This seems to indicate that the inaccuracies in the present boundary layer approach are magnified in the case of slender-ship theory. In this connection, it is of interest to note that in most previous studies, the boundary layer modifications have been used in conjunction with thin-ship theory.

Overall Trends

Except for the EP strut ($B/L = 0.15$), which is the fullest ship hull considered in the present study, the thin-ship values of C_W are generally higher than the corresponding slender-ship values, both with and without boundary layer effects. In some cases, the differences are quite small as in all the calculations for the thin Sharma strut ($B/L = 0.05$) or at the low Fn range for the Series 60 hull results including boundary layer effects. In the case of the EP strut, the slender-ship values are considerably higher than corresponding thin-ship values for $Fn > 0.5$.

The addition of δ^* serves generally, but not always, to reduce the value of C_W . Due to the larger streamline convergence effect for the R_V body, the reduction in C_W is generally larger for δ^* calculated using this body than for the R_W body. The exception occurs for the Series 60 hull, which has a non-vertical stern contour; this results in $R_W = 0$ at the stern end.

The values calculated by the present approach, without viscous effects, compare quite well with other similar approaches. The minor discrepancy in the case of the Series 60 hull is due to the use of quadrilateral panels in the present study and triangular panels in Ref. 47. Also, as required by theoretical considerations, the same value of C_W is obtained for the unsymmetrical TEP hull moving forward and backward in the absence of viscous effects.

Agreement with experimental data is erratic and, as may be expected, is largely dependent on hull shape. Generally, the slender-ship results are in relatively better agreement with experimental data than thin-ship values. Also, the addition of the boundary layer displacement thickness generally improves the agreement. In the case of the thin Sharma strut ($B/L = 0.05$), the theoretical calculations without viscous effects are in reasonably good agreement with experimental data. The addition of δ^* for the R_W body tends to improve the agreement, while δ^* for the R_V body tends to give too large a reduction in C_W and thus worsens the agreement. This may be due to the fact that the use of the R_V body tends to exaggerate the streamline convergence effect which may be largely absent on this deeply submerged strut. In the case of the Wigley hull, considering δ^* for both the R_W and R_V cases, the thin-ship values tend to either lie within the experimental range or bracket the upper limit; the corresponding slender-ship values either lie within the range or bracket the lower limit, which according to the data of Ref. 50, may be more applicable for the present case of a fixed model.

In the case of the full Series 60 hull ($B/L = 0.133$), which also has a flat bottom, the calculated results generally are much higher than the measured data for a fixed model. For this hull, it appears that the boundary layer correction alone is not sufficient to obtain reasonable agreement. Instead, the use of more complex wave resistance theories, such as low-speed theory or Guilloton's method, give improved agreement.

In the case of the unsymmetrical TEP hull, the calculated thin-ship results for both the R_W and R_V cases generally reproduce the experimental trend (obtained for other unsymmetrical hulls) for the difference in C_W between forward and backward motions. On the other hand, the slender-ship results do not reproduce this trend. This seems to indicate that inaccuracies in the boundary layer modeling tend to be magnified in the slender-ship case.

SUMMARY AND CONCLUSION

Calculation Approach

A relatively simple calculation procedure has been developed for obtaining the wave resistance, including viscous effects, on monohull ship forms. The procedure has been implemented as a computer program which runs well on a minicomputer, such as the Hewlett-Packard 1000.

The wave resistance calculations are made by using the direct thin-ship and zeroth order slender-ship theories. In these approaches, the source strengths are obtained directly from input hull geometry and do not require iterative procedures. The modification for viscous flow is obtained by adding the boundary layer displacement thickness δ^* to the actual ship hull. δ^* is calculated by approximating a double model of the actual hull by two equivalent axisymmetric bodies which respectively have volume (R_V body) and wetted area (R_W body) equal to those of the double model. Such an axisymmetric approach for making the boundary layer modification does not appear to have been previously tried in studies which model the effect of viscosity on wave resistance. The standard momentum integral equation is used to model the boundary layer growth along the axisymmetric bodies. It appears that δ^* calculated for the R_V and R_W bodies may bracket the actual boundary layer effect since they respectively tend to overemphasize and underemphasize the streamline convergence term which generally dominates boundary layer growth in the stern region. The pressure gradient on the body is calculated by using ordinary slender-body theory, modified by singularity gaps at the ends dependent on body nose radius and a simple iterative procedure to account for the boundary layer thickness in the stern region.

Hull Selection

The above procedure was used to calculate the wave resistance coefficient C_W over a range of Froude numbers Fn for five ship hulls: Wigley, Series 60 ($C_B = 0.60$), Sharma, (elliptic bow-parabolic stern) EP, and (thin EP) TEP. These hulls range in fullness ratio B/L from 0.05 to 0.15 and draft ratio H/L from 0.053 to 0.15. The first three hulls have extensive experimental data. The fourth was proposed for calculation for the Second DTNSRDC Workshop on Wave Resistance. The fifth hull was used mainly to indirectly compare the calculated trend in the difference between C_W for the hull in forward and backward motions with experimental data for other unsymmetrical hulls.

Six calculations of C_W were made at each Fn for the Wigley, Series 60, and Sharma hulls: thin- and slender-ship theories, each for the cases of no δ^* modification and δ^* calculated for the R_W and R_V bodies. For the EP hull, only results with no viscous effects are shown since the boundary layer calculations failed to converge for this form which is the fullest of the five. Ten calculations of C_W were made at each Fn for the TEP strut: thin- and slender-ship theories for the case of no viscous effects, and these two theories for δ^* using the R_W and R_V bodies for motion in the forward as well as backward directions.

Calculated Results

With the exception of the Series 60 hull which has a nonvertical stern contour, the value of δ^* at the stern end of the R_W axisymmetric body ranges from 1.1 to 1.7 times the flat plate value δ_{FP}^* . For the R_V axisymmetric body, the calculated value of δ^* is substantially larger, ranging from 3.4 to 8.4 times δ_{FP}^* . In many cases, the addition of this large value of δ^* results in a hull form which widens as the stern end is reached, which would give a source strength which has a sign opposite to that of original hull. In these cases, the new source strength is simply set equal to zero.

Many of the calculated trends are similar to those of previous studies. For example, in the absence of viscous effects, the thin-ship values of C_W are usually higher than corresponding slender-ship values. The notable exception occurs in the case of the fullest form EP hull, for which the slender-ship values are substantially higher for $Fn > 0.5$. This trend also generally holds when the δ^* effect is included; the effect of adding δ^* is to generally, but not always, reduce the value of C_W . With the principal exception of the previously mentioned case of the Series 60 hull, the reduction in the R_W case is usually smaller than that in the R_V case.

In the absence of viscous effects, the values calculated by the present approach are in excellent agreement with values calculated in other studies using comparable theories, for the Wigley, Sharma,

and EP hulls. The minor discrepancy in the case of the Series 60 hull is largely due to the use of quadrilateral panels in the present study and the use of triangular panels in the other study. Also in the absence of viscous effects, the present approach predicts the same values of C_W for the unsymmetrical TEP strut in forward and backward motions, as theoretically required.

In terms of agreement with experimental results, the slender-ship values are generally better than corresponding thin-ship values. Also, for either ship theory, the addition of δ^* generally improves the agreement. The agreement with experimental data for the individual hulls is erratic and, as may be expected, is dependent on hull shape. The agreement is generally good for the thin Sharma strut. The use of δ^* for the R_V body, which emphasizes the streamline convergence effect, somewhat worsens the agreement since this effect is relatively small for this deeply submerged hull for which a two-dimensional boundary layer approach may be more appropriate. For the Wigley hull, the use of slender-ship theory with δ^* for the R_W and R_V bodies gives results which tend to bracket the experimental values. Thus, for this hull, the use of a more accurate boundary layer model may give good agreement with experimental data for most Fn cases. The agreement in the case of the Series 60 hull is quite poor. Even in the case of the slender ship with δ^* modification, the calculated values are usually considerably higher than the appropriate experimental data. Results given at the First DTNSRDC Workshop on Wave Resistance indicate that the use of a more complex wave resistance theory, such as low-speed theory or Guilloton's method, brings substantially improved agreement.

In the case of the TEP strut, the thin-ship results using the δ^* correction for either the R_V or R_W body generally reproduce the experimentally observed trend (for other unsymmetrical hulls) for the difference between C_W for forward and backward motions. This trend is not reproduced by the slender-ship calculations. This seems to indicate that slender-ship theory is more sensitive to inaccuracies in the boundary-layer model than thin-ship theory.

REFERENCES

1. Michell, J.H., "The Wave Resistance of a Ship," *Philosophical Magazine*, Vol. 45, No. 272, pp. 106-123, January 1898.
2. Noblesse, F., "A Slender-Ship Theory of Wave Resistance," *Journal of Ship Research*, Vol. 27, No. 1, pp. 13-33, March 1983.
3. Newman, J.N., *Marine Hydrodynamics*, MIT Press, Cambridge, Massachusetts, 1977.
4. Eggers, K.W.H., Sharma, S.D., and Ward, L.W., "An Assessment of Some Experimental Methods for Determining the Wavemaking Characteristics of a Ship Form," *Transactions of the Society of Naval Architects and Marine Engineers*, Vol. 75, pp. 112-157, 1967.
5. Bai, K.J. and McCarthy, J.H. (ed.), *Proceedings of the Workshop on Ship Wave-Resistance Computations*, DTNSRDC, November 1979.
6. Chan, R.K.C., "Finite Difference Simulation of the Planar Motion of a Ship," *Proceedings of the Second International Conference on Numerical Ship Hydrodynamics*, pp. 39-52, September 1977.
7. Chan, R.K.C. and Chan, F.W.K., "Numerical Solution of Transient and Steady Free-Surface Flows about a Ship of General Hull Shape," *13th ONR Symposium on Naval Hydrodynamics*, pp. 257-280, October 1980.
8. von Kerczek, C.H. and Salvesen, N., "Numerical Solutions of Two-Dimensional Nonlinear Wave Problems," *10th ONR Symposium on Naval Hydrodynamics*, pp. 649-666, June 1974.

9. Salvesen, N. and von Kerczek, C.H., "Numerical Solution of Two-Dimensional Nonlinear Body-Wave Problems," *Proceedings of the First International Conference on Numerical Ship Hydrodynamics*, pp. 279-293, October 1975.
10. von Kerczek, C. and Salvesen, N., "Nonlinear Free-Surface Effects—The Dependence on Froude Number," *Proceedings of the Second International Conference on Numerical Ship Hydrodynamics*, pp. 292-300, September 1977.
11. Noblesse, F., "A Perturbation Analysis of the Wavemaking of a Ship, with an Interpretation of Guilloton's Method," *Journal of Ship Research*, Vol. 19, No. 3, pp. 140-148, September 1975.
12. Dagan, G., "A Method of Computing Nonlinear Wave Resistance of Thin Ships by Coordinate Straining," *Journal of Ship Research*, Vol. 19, No. 3, pp. 149-154, September 1975.
13. Hong, Y.S., "Numerical Calculation of Second-Order Wave Resistance," *Journal of Ship Research*, Vol. 21, No. 2, pp. 94-106, June 1977.
14. Chang, M.-S., "Computations of Three-Dimensional Ship-Motions with Forward Speed," *Proceedings of the Second International Conference on Numerical Ship Hydrodynamics*, pp. 124-135, September 1977.
15. Dawson, C.W., "A Practical Computer Method for Solving Ship-Wave Problems," *Proceedings of the Second International Conference on Numerical Ship Hydrodynamics*, pp. 30-38, September 1977.
16. Havelock, T.H., "Theory of Wave Resistance," *Proceedings of the Royal Society of London, Series A*, Vol. 138, pp. 339-348, October 1932.
17. Wehausen, J.V. and Laitone, E.V., "Surface Waves," *Encyclopedia of Physics*, Vol. 9, Springer-Verlag, Berlin, pp. 446-778, 1960.
18. Havelock, T.H., "Ship Waves: The Relative Efficiency of Bow and Stern," *Proceedings of the Royal Society of London, Series A*, Vol. 149, pp. 417-426, April 1935.
19. Wigley, W.C.S., "Comparison of Calculated and Measured Wave Resistances for a Series of Forms Not Symmetrical Fore and Aft," *Transactions of the Institution of Naval Architects*, Vol. 86, pp. 41-60, 1944.
20. Havelock, T.H., "Calculations Illustrating the Effect of Boundary Layer on Wave Resistance," *Transactions of the Institution of Naval Architects*, Vol. 90, No. 3, pp. 259-271, 1948.
21. Milgram, J.H., "The Effect of a Wake on the Wave Resistance of a Ship," *Journal of Ship Research*, Vol. 13, No. 1, pp. 69-71, March 1969.
22. Wigley, C., "Effects of Viscosity on Wave Resistance," *International Seminar on Theoretical Wave-Resistance*, Vol. III, pp. 1293-1310, 1963.
23. Wu, T.Y., "Interaction Between Ship Waves and Boundary Layer," *International Seminar on Theoretical Wave-Resistance*, Vol. III, pp. 1261-1291, 1963.
24. Himeno, Y., "Displacement Effect of Three-Dimensional Turbulent Boundary Layer and Wake of Ship," *International Seminar on Wave Resistance*, pp. 299-303, February 1976.

25. Kinoshita, T., "Viscous Effect on Waves of Thin Ship," *13th ONR Symposium on Naval Hydrodynamics*, pp. 693-706, October 1980.
26. Larsson, L. and Chang, M.S., "Numerical Viscous and Wave Resistance Calculations Including Interaction," *13th ONR Symposium on Naval Hydrodynamics*, pp. 707-728, October 1980.
27. Chapman, R.B., "Wave Resistance and Kelvin Wake of a Generalized Semisubmersible," Science Applications, Inc. Report SAI-77-980-LJ, December 1977.
28. Skop, R.A., Miner, E.W., and Judy, M., "KELGEN: A FORTRAN Program for Converting HULGEN Output to KELVIN Input," Encl. (1) to NRL ltr. 5844-108:RAS:mk of 11/9/83, November 1983.
29. Granville, P.S., "A Modified Froude Method for Determining Full-Scale Resistance of Surface Ships from Towed Models," *Journal of Ship Research*, Vol. 18, No. 4, pp. 215-223, December 1974.
30. Green, J.E., "Application of Head's Entrainment Method to the Prediction of Turbulent Boundary Layers and Wakes in Compressible Flow," Royal Aircraft Establishment Technical Report 72079, June 1972.
31. Wang, H.T., Dawson, C.W., and White, N.M., "Calculation of Streamlines on the USNS DUTTON," DTNSRDC Report SPD-771-01, May 1977.
32. Huang, T.T. and von Kerczek, C.H., "Shear Stress and Pressure Distribution on a Surface Ship Model: Theory and Experiment," *9th ONR Symposium on Naval Hydrodynamics*, pp. 1963-2010, August 1972.
33. von Kerczek, C., "Calculation of the Turbulent Boundary Layer on a Ship Hull at Zero Froude Number," *Journal of Ship Research*, Vol. 17, No. 2, pp. 106-120, June 1973.
34. Ludwig, H. and Tillmann, W., "Untersuchungen über die Wandschubspannung in turbulenten Reibungsschichten," *Ingenieur Archiv*, Vol. 17, pp. 288-299, 1949. (Also, NACA Technical Memorandum 1285, English translation, May 1950.)
35. Head, M.R., "Entrainment in the Turbulent Boundary Layer," Aeronautical Research Committee Reports and Memoranda No. 3152, September 1958.
36. Standen, N.M., "A Concept of Mass Entrainment Applied to Compressible Turbulent Boundary Layers in Adverse Pressure Gradients," AIAA Paper No. 64-584, 1964.
37. Granville, P.S., "Integral Methods for Turbulent Boundary Layers in Pressure Gradients," NSRDC Report 3308, April 1970.
38. García, J.M. and Zazurca, J.A.A., "Cálculo de la Resistencia Viscosa de un Buque a Partir de la de Cuerpos de Revolución Equivalentes," *Ingeniería Naval*, Vol. 44, No. 489, pp. 147-161, March 1976.
39. Joubert, P.N. and Matheson, N., "Wind Tunnel Tests of Two Lucy Ashton Reflex Geosims," *Journal of Ship Research*, Vol. 14, No. 4, pp. 241-276, December 1970.
40. Matheson, N. and Joubert, P.N., "A Note on the Resistance of Bodies of Revolution and Ship Forms," *Journal of Ship Research*, Vol. 18, No. 3, pp. 153-168, September 1976.

HENRY T. WANG

41. Hess, J.L. and Smith, A.M.O., "Calculation of Potential Flow About Arbitrary Bodies," *Progress in Aeronautical Sciences*, Vol. 8, Pergamon Press, New York, New York, 1967, pp. 1-138.
42. Karamcheti, K., *Principles of Ideal-Fluid Aerodynamics*, John Wiley and Sons, Inc., New York, New York, 1966.
43. Moran, J.P., "Line Source Distributions and Slender-Body Theory," *Journal of Fluid Mechanics*, Vol. 17, pp. 285-304, October 1963.
44. Wang, H.T. and Huang, T.T., "Calculation of Potential Flow/Boundary Layer Interaction on Axisymmetric Bodies," *Turbulent Boundary Layers*, ASME, New York, New York, pp. 47-57, June 1979.
45. Sharma, S.D., "Some Results Concerning the Wavemaking of a Thin Ship," *Journal of Ship Research*, Vol. 13, No. 1, pp. 72-81, March 1969.
46. Noblesse, F., "Introduction," *The Proceedings of the Second DTNSRDC Workshop on Ship Wave-Resistance Computations*, November 1983.
47. Scragg, C.A., "A Numerical Investigation of the Slender-Ship Wave Resistance Approximation," *The Proceedings of the Second DTNSRDC Workshop on Ship Wave-Resistance Computations*, November 1983.
48. Wigley, W.C.S., "Comparison of Calculated and Measured Wave Resistances for a Series of Forms not Symmetrical Fore and Aft," *Transactions of the Institution of Naval Architects*, Vol. 86, pp. 41-60, 1944.
49. Chen, C.Y. and Noblesse, F., "Preliminary Numerical Study of a New Slender-Ship Theory of Wave Resistance," *Journal of Ship Research*, Vol. 27, No. 3, pp. 172-186, September 1983.
50. Kajitani, H., Miyata, H., Ikehata, M., Tanaka, H., and Adachi, H., "The Summary of the Cooperative Experiment on Wigley Parabolic Model in Japan," *The Proceedings of the Second DTNSRDC Workshop on Ship Wave-Resistance Computations*, November 1983.
51. Noblesse, F., "Numerical Study of Eight Wave-Resistance Approximations," *The Proceedings of the Second DTNSRDC Workshop on Ship Wave-Resistance Computations*, November 1983.